Naval Research Laboratory

Washington, DC 20375-5320

NRL/MR/7322--20-10,152

Development of Embedded Two-way Nesting in the Navy Coastal Ocean Model

Jie Yu

Paul J. Martin

Timothy J. Campbell

Cheryl Ann Blain

Ocean Dynamics and Prediction Branch
Oceanography Division

September 18, 2020

REPORT DOCUMENTATION PAGE

Form Approved
OMB No. 0704-0188

1. REPORT DATE *(DD-MM-YYYY)*	**2. REPORT TYPE**	**3. DATES COVERED** *(From - To)*
18-09-2020	NRL Memorandum Report	

4. TITLE AND SUBTITLE

Development of Embedded Two-way Nesting in the Navy Coastal Ocean Model

5a. CONTRACT NUMBER

5b. GRANT NUMBER

5c. PROGRAM ELEMENT NUMBER

6. AUTHOR(S)

Jie Yu, Paul J. Martin*, Timothy J. Campbell, and Cheryl Ann Blain

5d. PROJECT NUMBER

5e. TASK NUMBER

5f. WORK UNIT NUMBER
6A56

7. PERFORMING ORGANIZATION NAME(S) AND ADDRESS(ES)

Naval Research Laboratory
4555 Overlook Avenue, SW
Washington, DC 20375-5320

8. PERFORMING ORGANIZATION REPORT NUMBER

NRL/MR/7322--20-10,152

9. SPONSORING / MONITORING AGENCY NAME(S) AND ADDRESS(ES)

Office of Naval Research
One Liberty Center
875 N. Randolph Street, Suite 1425
Arlington, VA 22203-1995

10. SPONSOR / MONITOR'S ACRONYM(S)

ONR

11. SPONSOR / MONITOR'S REPORT NUMBER(S)

12. DISTRIBUTION / AVAILABILITY STATEMENT

DISTRIBUTION STATEMENT A: Approved for public release; distribution is unlimited.

13. SUPPLEMENTARY NOTES

*Contractor

14. ABSTRACT

We report on the effort to implement and test embedded two-way nesting in the Navy Coastal Ocean Model (NCOM), which can run as a stand-alone ocean model, as well as a component within the Coupled Ocean/Atmospheric Mesoscale Prediction System (COAMPS). Details of the nesting procedure are documented, with particular attention on the feedback of the modeled fields from the child grid (fine mesh) to the parent grid (coarse mesh). The inconsistency between the 3D baroclinic velocities and the depth-integrated transports in the feedback is inherently due to the presence of bathymetry. This is addressed. The nesting procedure in NCOM is tested using simulations of idealized problems with well-defined solutions, and of real coasts with strong river-plume influences. Evaluations are made by comparing the results from one-way nested, two-way nested, and non-nested simulations. A preliminary comparison with field data is included. The two-way nesting procedure is shown to smoothly fuse the fine-mesh fields into the coarse-mesh ones, improving the consistency of the solutions on the different grids, especially in cases where the model results are sensitive to the grid resolution.

15. SUBJECT TERMS

16. SECURITY CLASSIFICATION OF:			**17. LIMITATION OF ABSTRACT**	**18. NUMBER OF PAGES**	**19a. NAME OF RESPONSIBLE PERSON**
					Jie Lu
a. REPORT	**b. ABSTRACT**	**c. THIS PAGE**	Unclassified Unlimited	41	**19b. TELEPHONE NUMBER** *(include area code)*
Unclassified Unlimited	Unclassified Unlimited	Unclassified Unlimited			(228) 688-5710

Standard Form 298 (Rev. 8-98)
Prescribed by ANSI Std. Z39.18

This page intentionally left blank.

CONTENTS

FIGURES

DEVELOPMENT OF EMBEDDED TWO-WAY NESTING IN THE NAVY COASTAL OCEAN MODEL

1. INTRODUCTION

The Navy Coastal Ocean Model (NCOM) was developed at NRL to meet the Navy's needs for coastal ocean simulation and prediction (Martin, 2000). It can run as a stand-alone ocean model, and has also been fully integrated into the Navy's Coupled Ocean/Atmospheric Mesoscale Prediction System (COAMPS), which uses the Earth System Modeling Framework (ESMF) to couple atmosphere, ocean, and wave models. While COAMPS provides a framework for one- and two-way coupling among atmosphere, ocean, and wave models, embedded coupling between coastal- and regional-scale ocean models is needed to advance their operational capability across multiple scales; in particular, in regions that are bathymetrically complex and strongly influenced by riverine, estuary, and wetland processes.

While unstructured grids offer the ability to locally vary their mesh size appropriate to the scales of the flow dynamics, the generation of unstructured grids can require some effort, and may not be as flexible as one desires. An efficient way to model multiscale dynamics in coastal oceans is to use embedding or nesting techniques, where a hierarchy of structured grids can interact with each other (e.g., Penven et al., 2006; Debreu and Blayo, 2008; Debreu et al., 2012; Haley and Lermusiaux, 2010). This gives greater flexibility, as structured grids of different mesh sizes can be placed as needed, and the same ocean model can independently run on each grid between the calls for grid-interactions. At present, NCOM has the fully operational capability of embedded one (1)-way nesting, where the child grids/nests (fine mesh, or FM) receive and update the boundary conditions/forcing by interpolating the newly available fields on the parent grid (coarse mesh, or CM). For two (2)-way interactions, the FM fields need to be fed back to the CM grid-points in the nested area via appropriate averaging operators. In this report, we document the recent implementation and testing of an embedded 2-way nesting procedure in NCOM.

This report is organized as follows. In Section 2, we first present background information regarding the model physics, the basic numerics, and the general aspects of the embedded nesting in NCOM. The implementation of the 2-way nesting is detailed in Section 3, where we discuss the origin of the inconsistency between the 3D baroclinic velocities and the depth-integrated barotropic transports in the feedback. An effective remedy is proposed. Testing cases are discussed in Section 4 for idealized physical problems, and in Section 5 for applications on real coasts, comparing the results from the nested and non-nested simulations. A preliminary comparison with field data is included. A summary follows in Section 6.

2. BACKGROUND

2.1 Model physics and basic numerics of NCOM

A brief description of NCOM is given here, while the details are referred to the literature (Martin, 2000; Barron et al., 2006). NCOM uses well-established ocean model physics and numerics. It is a free surface

Manuscript approved September 17, 2020.

model based on the primitive equations with the hydrostatic, Boussinesq, and incompressible approximations, and includes forcing with the atmospheric pressure and local tidal potential, source terms for river and runoff inflows, and quadratic bottom drag. It combines the numerical features in the Princeton Ocean Model (POM) and a sigma/z-level model developed at NRL, intending to provide flexibility and a user-choice of a number of established physical and numerical parameterizations/schemes (e.g., the horizontal and vertical mixing models, advection, open boundary conditions, etc). The model equations are discretized with finite differences in flux-conservative form on an Arakawa C-grid. Leapfrog in time is used with an Asselin filter. The horizontal grid is orthogonal, curvilinear as in POM. The vertical grid uses sigma coordinates in the upper layers in order to follow the movement of the free surface, and z-levels in the lower layers. The depth at which the grid changes to the z-levels is specified by the user. The vertical grid can be set up with sigma layers all the way to the bottom in order to be terrain-following at all depths. The option to use a generalized vertical coordinate is also provided. The propagation of surface waves and vertical mixing are treated implicitly. The capability for wetting and drying of the grid cells is implemented and validated (Martin et al., 2015).

2.2 General aspects of embedded nesting in NCOM

NCOM's code structure was designed to facilitate the use of nesting, i.e., almost all the model variables are passed through the argument lists of the subroutines so that the same code can be used for different grids/nests. Each grid/nest has its own separate input and output files that all have the same format. This is not always the most convenient, but it is simple and flexible since parameters and forcing can be individually specified for different grids.

The setup programs have some routines to make setting up nests easier. The main grid is set up by a call to subroutine *mainset*, which generates all the input files needed for the main grid. The subroutine *nestset* is then called for each nested/child grid. Subroutine *nestset* can read the input files that have been generated for the parent grid in which the nest is embedded to allow interpolation of the FM fields from the values on the CM. Alternatively, fields can be directly interpolated to the FM from the databases used by the CM, or from a different source.

Some current restrictions on nesting are mentioned. (1) The vertical grids must match, though the child grid may have fewer vertical levels if the domain is shallower than the parent grid such that the deeper levels on the FM would just be land points. (2) The CM and FM must be aligned. (3) The nesting ratio (i.e., the number of FM cells per CM cell) must be an integer.

Theoretically speaking, any number of nests can be embedded within a given grid/nest. The parameter file for each nest (OPARM_#.D) contains the number of the grid in which the nest is embedded, the location of the nest within its parent grid, and the nesting ratio. There is no explicit restriction on the grid-nesting ratio or time-step ratio between the child and parent grid, and the two ratios need not be the same. For 2-way nesting, however, the grid ratio should probably be limited to 3:1. For Arakawa C-grids, 3:1 is the minimal ratio such that every CM point inside the nested area is co-located with a FM point. This tends to give the optimal consistency when feeding the FM fields back to the CM, while larger ratios cause too strong a contrast of the scales resolved to benefit a smooth, strong coupling between the grids (Debreu and Blayo, 2008).

Since each nest/grid has its own input files, specific barotropic tidal forcing can be applied to the open boundary of an individual nest, which will then be superimposed on the boundary conditions taken from

the parent grid. This allows tidal forcing on a child grid to be different from that on the parent grid. This feature is particularly convenient in nearshore simulations where complex bathymetry and strong nonlinear interactions can generate additional tidal constituents on a nest that are not being forced on the boundary of the much larger domain of the CM.

Time integrations on the parent grid and nest(s), interpolation of the boundary conditions for the child grid from the parent grid, and feeding the FM fields back to the parent grid, are all handled automatically by NCOM during the model run.

2.2.1 Correspondence of indexes on the CM and FM

The location of the lower-left corner of the nest on the CM is (i_s, j_s). Note that this CM cell contains FM point $(2,2)$, but not FM point $(1,1)$, which is on the boundary of the FM. Let a be the grid ratio. The indexes (i_1, j_1) on the CM are converted to the real indexes (x_2, y_2) on the FM, where

$$x_2 = (i_1 - i_s)a + (a+3.0)/2.0, \quad y_2 = (j_1 - j_s)a + (a+3.0)/2.0. \tag{1}$$

In reverse, the FM indexes (i_2, j_2) are converted to the real indexes (x_1, y_1) on the CM, where

$$x_1 = i_s + i_2/a - (a+3.0)/(2a), \quad y_1 = j_s + j_2/a - (a+3.0)/(2a). \tag{2}$$

2.2.2 Bathymetry setup

The bathymetry for a nest can be made to be consistent with that on the parent grid (in the sense that the FM and CM depths are same at the co-located grid points), or refined in the interior of the nest, e.g., being interpolated from a higher resolution database (or directly from the original data source used for the CM). Obviously, having a point-wise consistent depth does not imply the identity of the CM and FM bathymetries (as continuous functions). Subroutine *nestset* provides the option to refine the FM bathymetry by 'blending' the interpolation from the CM with a higher resolution database, while keeping the needed bathymetry-consistency near the open boundary of the nest. For each grid, NCOM uses both 2D and 3D arrays to mask the land/sea points at the cell centers, as well as at the velocity points on the cell faces. The mask variable is binary (1/0 for sea/land).

Near the open boundary of a nest, the following bathymetry rules apply. (i) *Setting the land-sea mask*: If the land-sea mask on the CM does not change crossing the FM boundary, the same CM mask is assigned to the FM boundary points there. If the CM has a land cell on one side and a sea cell on the other side of the FM boundary, the FM boundary points there are land. (In the case where the CM sea cell is outside and land cell inside the FM boundary, the inflow would be blocked, making the FM boundary points necessarily land.) (ii) *Setting the depths:* For the sigma layers, linear interpolation of the CM depths is used near the FM boundaries. This allows a change in depth across the open boundary. For the z-levels, we use the same depth on the FM boundary point as for the CM cell in which the FM point lies. If the CM has a sea cell inside the FM boundary and a land cell just outside (at the same vertical level), the FM should be shallow in the same way. But, if the CM has a land cell inside the FM boundary but a sea cell outside (at the same vertical level), the FM should maintain the same depth across the boundary. (The FM could not use this CM sea cell since the flow just runs into a wall.) At the transition from sigma layers to z-levels, if there is a z-level

cell below z_w (the user-specified depth of transition), we set the depth h_u at a u-point as $h_{uf} = h_{uc} = z_w$, where the subscripts f and c indicate associations with the FM and CM, respectively. Otherwise, we set $h_{uf} = h_{uc} = (h_c(l-1) + h_c(l))/2$, where h_c is the depth at the CM cell center and l is the layer number increasing downward. The depths at v-points are similarly set. While it is allowed by the rules, it is in general desirable to avoid large changes in depth across the open boundary of the FM. The rules specified above are similarly applied when interpolating the CM bathymetry onto the interior FM points of the nest.

When the FM bathymetry is refined using a higher resolution data source, one has the option to update the CM bathymetry using the average of the FM depths. This is done for the CM points in the interior of the nest, excluding those near the boundary. This supposedly improves the consistency of cell-integrated quantities on the CM and FM in the 2-way nesting (e.g., Haley and Lermusiaux, 2010). The following rules apply when updating the CM bathymetry, assuming a 3:1 grid ratio. (i) If all 9 FM points within a CM cell are masked as the land/sea, the CM cell is updated as a land/sea point accordingly. (In regions where the bathymetry is highly complex, it is possible that all FM center points within a CM cell are masked as the land (or sea), yet the CM cell-center is masked otherwise based on the initial bathymetry setup.) (ii) If 5 or more FM points are sea points, the CM cell is a sea point. Otherwise, the CM cell is made a land point. When z-levels are used, the bathymetry is rounded off to the nearest z-level. As a results, updating the CM bathymetry using the FM-average can become ineffective at some grid points because the round-off procedure can overwrite the corrections made.

3. TWO-WAY NESTING PROCEDURE IN NCOM

The discussion here is based on a grid-nesting ratio of 3:1. There is no vertical mesh refinement in the present implementation. The time-stepping refinement factor is the same as the grid-nesting ratio. NCOM runs independently on the parent grid and the nest(s). Exchange of information, i.e., grid interaction, occurs upon finishing one time-step of integration on the CM and three time steps on the FM when the fields have been advanced to the same time level. The boundary forcing for the FM is updated by interpolating the CM fields at the current time level to the dynamic interfaces (see below). The CM fields on the points in the interior of the nest, with the outer limits specified by the feedback interfaces, are updated using the appropriate averages of the FM fields at the current time level. The next cycle of time integration then begins on each grid.

The interpolation of the CM fields to the FM boundary is the procedure used for 1-way embedded nesting, and has been implemented and validated in previous efforts. It is briefly summarized here. The CM fields are linearly interpolated to the FM open boundaries. Near the land-sea boundary of the FM, linear (mild) extrapolation is applied and constrained by the conditions that (i) the FM surface elevation η has a zero gradient along the boundary, and (ii) the FM barotropic tangent velocity and baroclinic tangent velocity both have zero values.

The algorithms/schemes of feeding back the FM fields have been the focus of a number of studies (e.g. Debreu and Blayo, 2008; Haley and Lermusiaux, 2010). We select from those existing schemes, while trying to minimize the complexity of the code implementation and modification and to not compromise the performance of the grid-coupling. Our feedback strategy is described, as follows.

3.1 Separation of the feedback and dynamic interfaces

The existing studies on embedded nesting methods in atmospheric and oceanic modeling show that this separation is in general necessary (e.g., Debreu and Blayo, 2008; Debreu et al., 2012). Appropriate

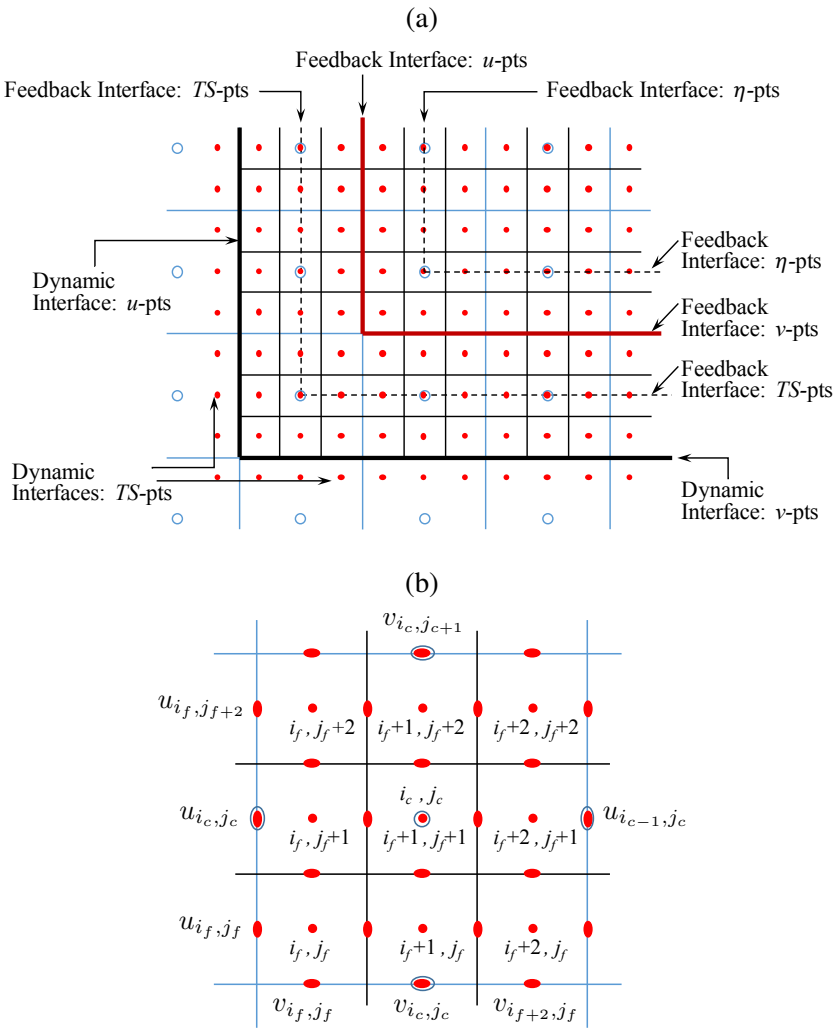

Fig. 1—(a) A schematic illustration of a portion of two embedded nesting grids with a mesh size ratio of 3:1, showing the dynamic interfaces (where the boundary forcing for the FM is updated by interpolating the CM fields) and the feedback interfaces (i.e., the outer limits within which the CM fields in the interior of the nest are updated using the appropriate averages of the FM fields). Solid dots and open circles are, respectively, the centers of the FM and CM cells, where the scalars (e.g., T, S, η) are stored. (b) A CM cell being divided into 9 FM cells, showing the velocity points. The vertical and horizontal ellipses are for u and v, respectively. Open symbols are on the CM.

separation can suppress the noise-production near the dynamic interfaces due to the interpolations, and reduce the inconsistency that may arise due to applying both interpolation and feedback operators on the same set of CM points (see the review discussion in Debreu and Blayo, 2008). We have explored various arrangements of placing the feedback interfaces (relative to the dynamics interfaces) and concluded that the optimal arrangement for NCOM is as indicated in Fig. 1a. The feedback interfaces for the 3D baroclinic velocities u and v are placed inward of the nest, being one CM-cell away from the respective dynamic interfaces (which are also the physical boundaries of the nest). The depth-integrated 2D barotropic transports use the same feedback interfaces as for u and v. For the temperature T and salinity S, the feedback interface is defined by the centers of the first CM cells (inside the nest) along the physical boundary of the nest.

However, it is better to place the feedback interface for the surface elevation η on the inner side of the velocity feedback interfaces, being one CM cell away from the feedback interface for T and S.

3.2 Feedback (averaging) operators

The CM fields are replaced/updated by the appropriate averages of the FM fields, layer-by-layer, within the limits specified by the corresponding feedback interfaces. For a scalar $r = T$, S or η, the average of 9 FM points within the CM cell is used, i.e.,

$$\begin{aligned} r_{i_c,j_c} &= \tfrac{1}{9}\left[\left(r_{i_f,j_f}+r_{i_f+2,j_f+2}\right)+\left(r_{i_f,j_f+2}+r_{i_f+2,j_f}\right)\right. \\ &\quad \left.+\left(r_{i_f,j_f+1}+r_{i_f+2,j_f+1}\right)+\left(r_{i_f+1,j_f}+r_{i_f+1,j_f+2}\right)+r_{i_f+1,j_f+1}\right], \end{aligned} \tag{3}$$

where the arrangement of indexes refers to Fig. 1b. The indexes for the time and the vertical layer are suppressed for clarity. The sequence of calculations written in (3) is to enforce an 8-fold symmetry.

For the 3D baroclinic velocities, the simple 3-point averages are

$$u_{i_c,j_c} = \tfrac{1}{3}\left[\left(u_{i_f,j_f}+u_{i_f,j_f+2}\right)+u_{i_f,j_f+1}\right], \tag{4a}$$

$$v_{i_c,j_c} = \tfrac{1}{3}\left[\left(v_{i_f,j_f}+v_{i_f+2,j_f}\right)+v_{i_f+1,j_f}\right]. \tag{4b}$$

Debreu et al. (2012) suggests that a higher-order operator, which is a weighted average involving 9 FM velocity-points, can lead to improvement since it produces a stronger damping of small-scale noise. The weighted averages are

$$u_{i_c,j_c} = \tfrac{1}{9}\left[\left(u_{i_f,j_f-1}+u_{i_f,j_f+3}\right)+2\left(u_{i_f,j_f}+u_{i_f,j_f+2}\right)+3u_{i_f,j_f+1}\right], \tag{5a}$$

$$v_{i_c,j_c} = \tfrac{1}{9}\left[\left(v_{i_f-1,j_f}+v_{i_f+3,j_f}\right)+2\left(v_{i_f,j_f}+v_{i_f+2,j_f}\right)+3v_{i_f+1,j_f}\right]. \tag{5b}$$

The depth-integrated 2D barotropic transports are fed back using the same operators as for the 3D u and v. We have tested both operators, (4) and (5), in the series version of NCOM, and found that the differences are insignificant. Thus, we opted for the simple 3-point average (4) in the latest version of NCOM.

For clarity, the land-sea masks appropriate to the FM field variables are suppressed in (3)–(5), i.e., as if all the points are sea points. In coding, the land-sea masks are used so that the averaging is just over the FM sea points.

3.3 Bathymetry discrepancy and correction of the 3D baroclinic velocities

The bathymetries represented on the CM and FM cannot be identical, because of the different grid resolution. Despite the effort to improve the consistency of the bathymetries when setting up the grids (see Section 2.2.2), there remains inconsistency when feeding the 3D baroclinic velocities and depth-integrated barotropic transports back to the CM. This is because the calculations of depth integration and grid-point average are not inter-changeable. Consider the simple average over 3 FM u-points where the depths are

$z = -h_1, -h_2, -h_3$ and the surface elevations are $\eta = \eta_1, \eta_2, \eta_3$. (The subscript f for the FM is suppressed here.) The depth-integrated transport is defined as

$$U = \int_{-h}^{\eta} u(x,y,z)\mathrm{d}z. \tag{6}$$

The 3-point average of U is

$$\langle U \rangle = \tfrac{1}{3}\left(U_1 + U_2 + U_3\right) = \tfrac{1}{3}\left(\int_{-h_1}^{\eta_1} u_1\,\mathrm{d}z + \int_{-h_2}^{\eta_2} u_2\,\mathrm{d}z + \int_{-h_3}^{\eta_3} u_3\,\mathrm{d}z\right). \tag{7}$$

The updated barotropic transport $U_c = \langle U \rangle$ is applied at the CM u-point (co-located at the FM point 2), where the baroclinic velocity is updated to $u_c = \langle u \rangle = \frac{1}{3}\left(u_1 + u_2 + u_3\right)$, according to the feedback procedure. If we calculate the transport directly from the newly updated baroclinic velocity, it would be

$$\int_{-h_c}^{\eta_c} u_c\,\mathrm{d}z = \tfrac{1}{3}\int_{-h_c}^{\eta_c} \left(u_1 + u_2 + u_3\right)\mathrm{d}z, \tag{8}$$

where h_c and η_c are, respectively, the depth and surface elevation at the CM point in question. It is clear that the calculations in (7) and (8) are not the same, i.e., $\langle U \rangle \neq \int \langle u \rangle \mathrm{d}z$, even if we make the CM depth same as the FM depth at the co-located point (i.e., $h_c = h_2$), and exclude the contribution of surface elevation in the depth integration.

This is an inherent inconsistency when the 3D baroclinic velocities and 2D barotropic transports are both fed back to the CM. Directly feeding back the latter is desirable so that the mass fluxes are consistently represented on the CM and FM. An expedient remedy is to correct the 3D velocities u and v to match the barotropic transports upon feeding them back to the CM. Evenly distributing the difference between (7) and (8) over the depth, we obtain a small amount of velocity correction Δu. We adjust the 3D velocity to $u_c = \langle u \rangle + \Delta u$, layer-by-layer, so that $\int u_c\,\mathrm{d}z = \langle U \rangle$ at the CM points receiving the feedback. The v-velocity is corrected following a similar procedure. Considering that feeding back the FM fields is, in effect, perturbing the CM fields, it is not unreasonable to slightly adjust the baroclinic velocities u and v so that the perturbations are consistent in some sense. The proposed remedy also conforms to the general numerical procedures (unrelated to grid nesting) in NCOM, which checks and corrects the 3D velocity field to match the depth-integrated transport field at each time step on each grid. It is evident from our tests that the proposed remedy is effective to correct the bathymetry-induced inconsistency when updating the CM velocity fields: In the idealized tests (Section 4) where the water depth is constant, the differences in the results are found to be slight and insignificant with or without correcting the 3D u, v upon feeding back to the CM in the 2-way nesting, as expected. However, in the simulations on real coasts (Section 5) where the bathymetry is highly variable, if the correction of the 3D u, v is turned off in the 2-way nesting, the Courant-Friedrichs-Lewy (CFL) condition for the vertical advection can become very large at some points on the CM almost immediately after the feedback procedure is called. Once the correction of the 3D u, v is turned on, the CFL violation disappears.

3.4 The simplified vs. full two-way nesting

For some large-scale flows, the momentum budget is approximately in geostrophic balance, i.e., the velocity field primarily evolves according to $\boldsymbol{f} \times \boldsymbol{v} = \nabla p(\rho)/\rho$, where $\boldsymbol{f}$ is the Coriolis parameter, and ρ

and p are the density and pressure fields. Depending on the modeling purposes, it may be sufficient in physics, and computationally economic, to feed only the FM scalar fields T and S back to the parent grid, and not the FM velocity field. This assumes that the CM velocity field will be indirectly updated through the density field when the equation of state is computed using the newly updated T and S because of the geostrophic balance. To provide modeling flexibility and test the sensitivity of the two-way coupling, we provide a user-selectable choice to turn on/off the feedback of selected FM variables. In the following discussions, the term *simplified two-way nesting* refers to the simulations in which only the FM T and S are fed back to the parent grid. In a *full two-way nesting*, the 3D baroclinic velocities, the 2D barotropic transports, the surface elevation, as well as T and S, are all fed back from the FM to the CM.

4. IDEALIZED EXPERIMENTS

To test and evaluate the implementation of the 2-way nesting schemes, we first set up NCOM simulations of idealized problems. Two cases are discussed here. The result of a non-nested simulation on a single grid is referred to as a reference solution and used for comparison. Note that the result on the CM in the 1-way nesting is also the coarse-resolution reference solution, while the high-resolution reference solution is on a single grid of mesh size the same as that used on the nest.

4.1 Eastward propagation of an equatorial Kelvin wave

This case is primarily set up to show that, despite the crude assumption, the simple 2-way nesting strategy of feeding back only T and S can, to some degree, improve the large-scale structure of the CM velocity field when geostrophic balance approximately holds. The physical problem was previously used by Rowley and Ginis (1999) to demonstrate their moving nesting scheme in a 1.5-layer, reduced-gravity ocean model. The Kelvin wave is generated by a local perturbation of the thermocline. Atmospheric forcing at the sea surface is absent. The Kevin wave steepens as it propagates eastward without dispersion, and develops interesting structures (e.g., the resolution-limited, sharp wave front) that are useful to test the numerics. In our setup, a mesh size of 60 km and a time step of 5400 s are used on the parent grid. The vertical grid consists of 30 sigma layers with the layer-thickness increasing log-linearly from $z = 0$ to $z = -2000$ m. The initial conditions are zero velocity, constant $S = 35$ psu, and $T(z)$ corresponding to the Levitus climatology for the equatorial Pacific at 180E, which is superimposed with a perturbation for the Kevin wave. The Gaussian-shaped temperature perturbation has a horizontal scale of 500 km and a maximum at $z = -180$ m. The maximum of the perturbation is 4°C, which corresponds to amplitude of -60 m in the initial perturbation of the layer thickness in Rowley and Ginis (1999). The initial perturbation generates an eastward-propagating Kelvin wave, as well as small amplitude, westward-propagating Rossby waves (Philander et al., 1984).

In the absence of bathymetry, the zonal velocity u of the eastward-propagating Kelvin wave is approximately in geostrophic balance with the north-south pressure gradient. On the CM, the SSH is visibly improved in the simplified 2-way nesting that feeds back only the FM T and S but not the velocities, showing the sharp wave front that resembles the high-resolution reference solution (compare Fig. 2a and Fig. 2c). In the 1-way nesting (Fig. 2b), the parent grid does not receive any information from the FM nest, and thus shows a slightly less focused wave front, which is simply a feature of the coarse-resolution reference solution. The major differences in the velocity fields are seen in the near-zero contours (noise level). The result of the full 2-way nesting (not shown) is little different from that of the simplified 2-way nesting, confirming the expectation that it is less important to directly feed the velocity field back to the CM when the flow dynamics are dominantly controlled by the geostrophic balance. As the Kelvin wave leaves the nest,

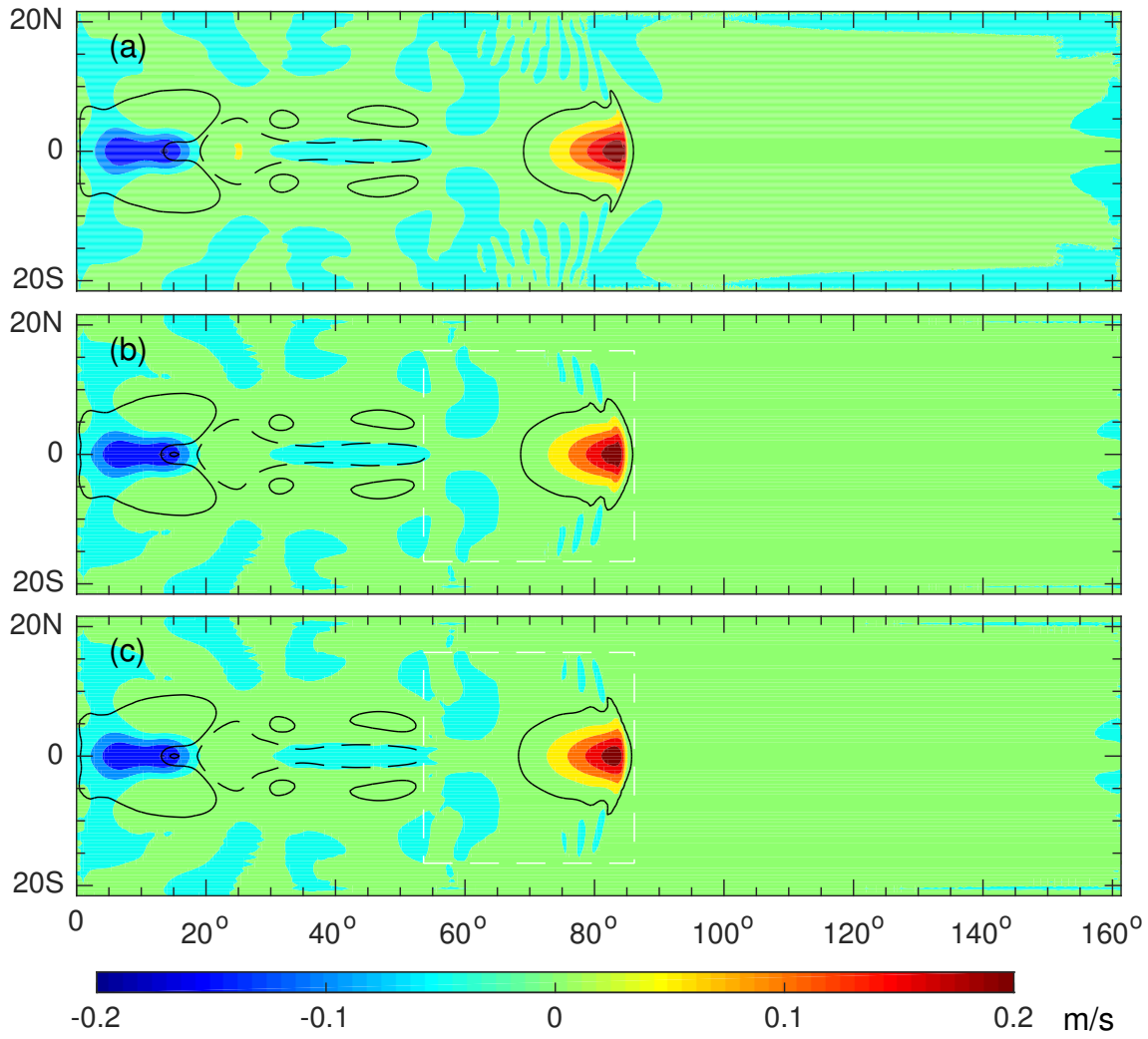

Fig. 2—The zonal velocity u (shade) at $z = -181$ m, showing the eastward propagation and steepening of the Kelvin wave at 1200 hr on day 26: (a) the high-resolution (of 20 km) reference solution on a single grid; (b) the solution on the CM in the 1-way nesting (which is also the coarse-resolution (of 60 km) reference solution); (c) the solution on the CM in the simplified 2-way nesting. Superimposed are the contour lines of SSH (solid for 0.005 m; dashed for -0.005 m), indicating the regions of high and low pressure. The flat bed is at $z = -2000$ m. In (b) and (c), the dashed box shows the nested area.

small-scale, westward-propagating waves are generated at the eastern boundary of the nest (Fig. 3). While these reflected waves are due to the imperfection of the numerical open boundary conditions (hence would not be wanted to be fed back to the CM), it is interesting to note that their presence on the FM is much more suppressed in the simplified 2-way nesting, compared to that in the 1-way nesting (compare Fig. 3b and Fig. 3d). Due to the two-way grid-interaction, the solutions on the CM and FM are more consistent. As a result, the back-scattering (reflection) of the wave at the open boundary is reduced. NCOM provides several options for the numerical open boundary conditions, from which a user can choose independently for the scalar fields, the surface elevation, and the velocities on each grid. The reflected waves at the FM boundary cannot be completely eliminated by the numerical open boundary conditions that are prescribed,

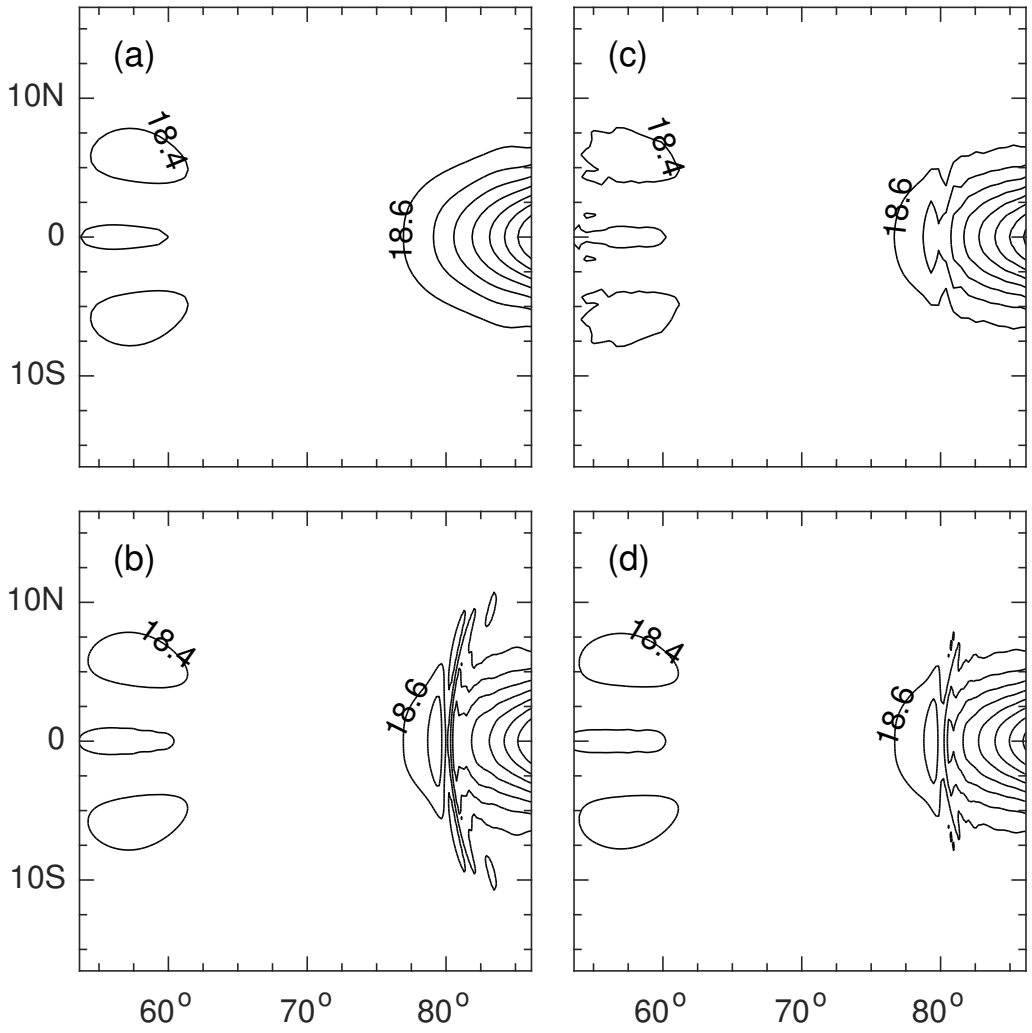

Fig. 3—The temperature filed at $z = -181$ m under the eastward-propagating Kevin wave, comparing the results in the 1-way nesting (left panels) and the simplified 2-way nesting (right panels): (a) and (c), T on the CM in the nested area; (b) and (b), T on the FM. The time is at 1200 hr on day 30 when the wave is leaving the nested area. The contour interval is 0.2°C.

though some options better suppress the reflection than others. They are similarly seen in the reference solution as the Kelvin wave exits the eastern boundary of the model domain (thus are not due to the feedback procedure), and are clearly resolution-dependent (Fig. 4). This shortcoming may be corrected by adding a sponge layer near the open boundary, in which an artificially large damping is employed to prevent the disturbance/noise from propagating back into the nest or model domain (Debreu et al., 2012).

4.2 Evolution of a baroclinic vortex

This idealized problem has been used by various authors to test and evaluate the performance of embedded 1-way and 2-way nesting in ocean models (e.g., Spall and Holland, 1991; Penven et al., 2006; Debreu et al., 2012) and, hence, may be regarded as a benchmark test. A theoretical study of the physical problem can be found in McWilliams and Flierl (1979). We set up this experiment closely following the previous studies.

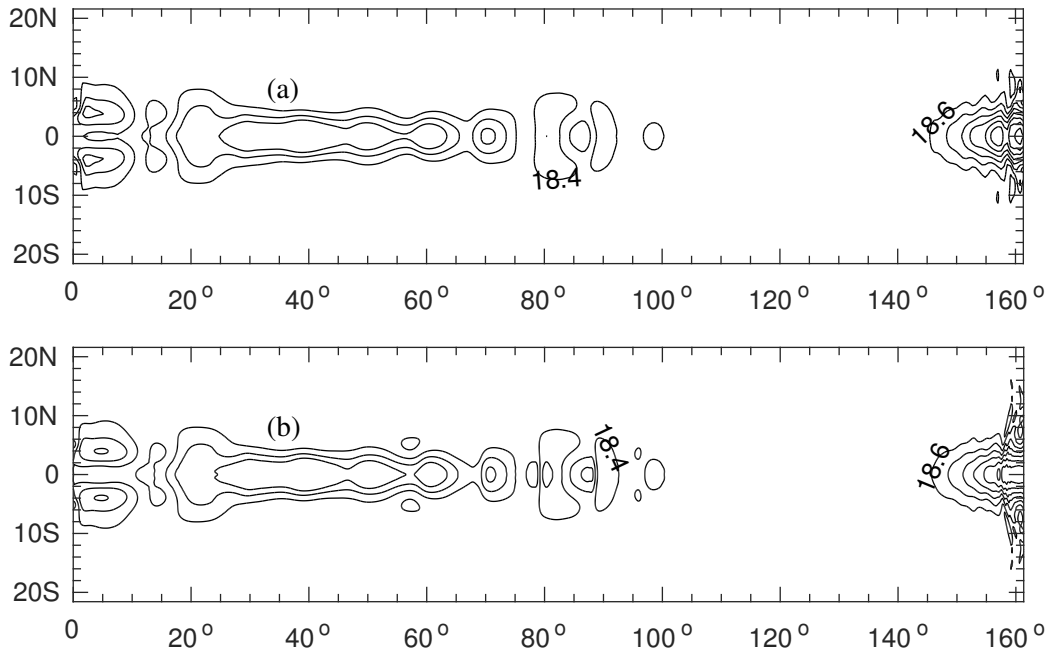

Fig. 4—The reference solution (non-nested simulation on a single grid) of T at $z = -181$ m on day 64, showing the resolution-dependent reflection at the eastern boundary when the Kelvin wave exits the model domain: (a) the low resolution (of 60 km); (b) the high resolution (of 20 km).

An initially axisymmetric vortex is centered at 38.5N, 38.5E in a square basin with a uniform depth of 5000 m, and corresponds to a Gaussian pressure distribution, which has a maximum geostrophic velocity of 1 m/s and a horizontal *e*-folding scale of 60 km at the surface. The function describing the pressure perturbation is slightly modified from that in Penven et al. (2006) and Debreu et al. (2012) so that the function and its first derivation in z are continuous (see Appendix A). The initial horizontal velocity field is in geostrophic balance with the horizontal pressure gradient. The parent grid uses a horizontal mesh size of 30 km and time step of 600 s. The nest is at the center and covers the initial vortex. Following Penven et al. (2006) and Debreu et al. (2012), we use ten evenly-spaced vertical layers and turn off the horizontal and vertical diffusion (viscosity), and bottom friction. Recall that the surface layer is always within the sigma coordinate in NCOM. There is no atmospheric or the tidal forcing.

The evolution of the vortex is dominated by its southwestward propagation under the Coriolis effect, leaving behind a wake. The anticyclonic vortex approximately maintains its shape as it propagates and slowly weakens in strength due to the generation of the wake (see the sea surface temperature SST of the high-resolution reference solution in Figs. 5a – 5c). In contrast, in a coarse-resolution simulation, the vortex deforms, rapidly loses its strength, and becomes increasingly westward propagating as time goes on (see the CM solution in the 1-way nesting in Figs. 5d – 5f). The CM solution is significantly improved in the full 2-way nesting due to feeding back the FM fields, with the vortex structure and the wake closely resembling the high-resolution reference solution up to $t = 60$ days (Figs. 5g – 5i). The discrepancy in the orientation of the vortex becomes more noticeable (compare Fig. 5h and Fig. 5b). For $t > 60$ days, the vortex is outside the nested area, and the FM nest mostly resolves the wake flow. Consequently, feeding back the FM fields becomes less effective in influencing the vortex propagation, and the CM solution begins to show the features

of the coarse-resolution reference solution; for instance, the weakened vortex and the tendency to propagate west (compare Fig. 5c, Fig. 5f, and Fig. 5i).

While it is used to compute the initial velocity field, the geostrophic balance is not expected during the evolution of the vortex. For comparison, we have included the result from the simplified 2-way nesting (Figs. 5j – 5l). During the short-term evolution ($t < 30$ days), the vortex and the wake on the CM are very similar to the high-resolution reference solution, and much better resolved compared with the coarse-resolution reference solution (Fig. 5d). This presumably is because the flow is still under the influence of the initial condition, which is in geostrophic balance. For $t > 30$ days, however, the vortex structure on the CM rapidly degenerates, as the ageostrophic flow develops, signifying the failure due to the lack of feeding back the FM velocity fields.

The sea surface zonal velocity SSU and sea surface height SSH on the CM are shown in Fig. 6 for the nested area, comparing different simulations. The corresponding results of SSU and SSH on the FM nest are in Fig. 7. In the full 2-way nesting, the solutions on the CM and FM are consistent, and both similar to the high-resolution reference solution (compare Fig. 6g and Fig. 7d for $t = 30$ days, and Fig. 6h and Fig. 7e for $t = 60$ days). In comparison, there is a greater discrepancy between the CM and FM solutions in the 1-way nesting; in particular, when the CM solution is no longer accurate enough to represent the truth (e.g., for $t > 60$ days), the FM solution has also significantly departed from the high-resolution reference solution because of the inaccurate boundary forcing obtained from the CM (compare Fig. 6d and Fig. 7a for $t = 30$ days, and Fig. 6e and Fig. 7b for $t = 60$ days). In the simplified 2-way nesting, a considerable inconsistency is also observed between the CM and FM solutions (compare Fig. 6j and Fig. 7g for $t = 30$ days, and Fig. 6k and Fig. 7h for $t = 60$ days).

As the horizontal structure of the flow is improved, so is the vertical structure, even though there is no vertical mesh refinement. It is seen in Fig. 8 that the vertical fluctuation of T on the CM given by the full and simplified 2-way nesting both show better agreement with the high-resolution reference solution, compared with that given by the 1-way nesting. This is consistent with the results in Fig. 5. At later times (e.g., $t = 60$ days), the vertical fluctuation of T on the CM in the 1-way nesting becomes much less depth-penetrating due to the weakened vortex strength, as well as the dislocation of the vortex center (being away from that in the high-resolution reference solution).

If the high-resolution reference solution is taken as the 'truth', the root-mean-square (RMS) errors of the model variables can be computed. The RMS errors of SST, SSH, and SSU on the CM are compared among the different simulations in Fig. 9. For $t < 60$ days when the vortex is inside the nested area, feeding back the FM fields is effective and reduces the errors in the CM fields; although the errors in SST are similar, with or without feeding back the FM velocity fields, the errors in SSH and SSU are considerably greater in the simplified 2-way nesting. For $t > 60$ days, the RMS errors in the full 2-way nesting suddenly elevate as the vortex leaves the nested region, and these errors remain the greatest. This, however, should not be interpreted that the full 2-way nesting becomes inferior to the others, as we have seen in Fig. 5 that at $t = 100$ days it still resolves the vortex strength and shape better than the other nested simulations. The apparent elevation of the errors in the full 2-way nesting is largely due to the dislocation of the vortex center (compare Fig. 5c and Fig. 5i) that is caused by the tendency of the westward propagation on the CM as the influence of the nest wanes. On the contrary, the RMS errors on the CM in the 1-way nesting plateau for $t > 70$ days, as the vortex degenerates due to the insufficient resolution.

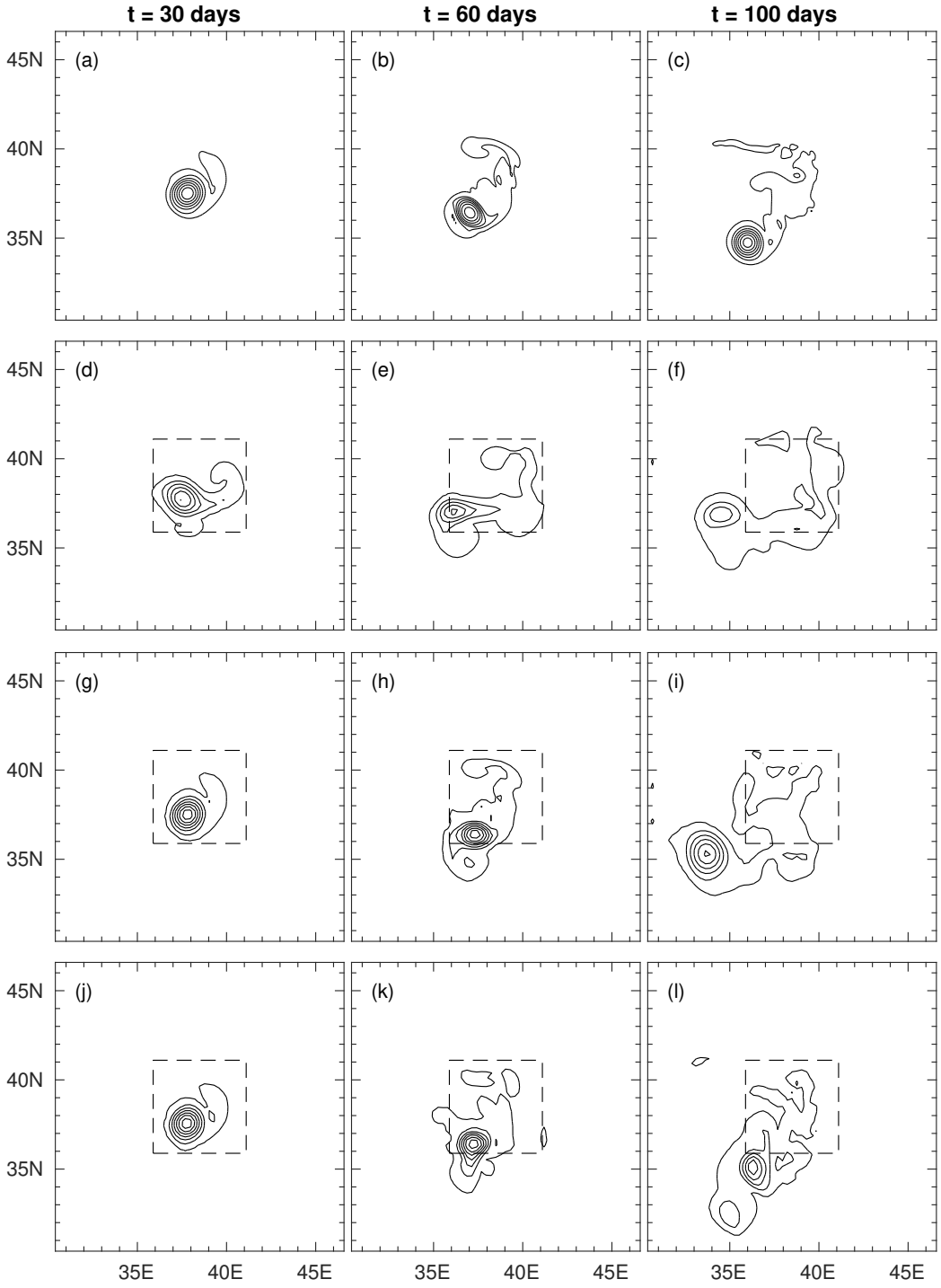

Fig. 5—SST as the baroclinic vortex evolves: (a-c) the high-resolution (of 10 km) reference solution; the solution on the CM in (d-f) the 1-way nesting (also the 30-km reference solution), (g-i) the full 2-way nesting, and (j-l) the simplified 2-way nesting. The contour interval is 0.3°C, increasing from 17.9°C towards the maximum at the vortex center.

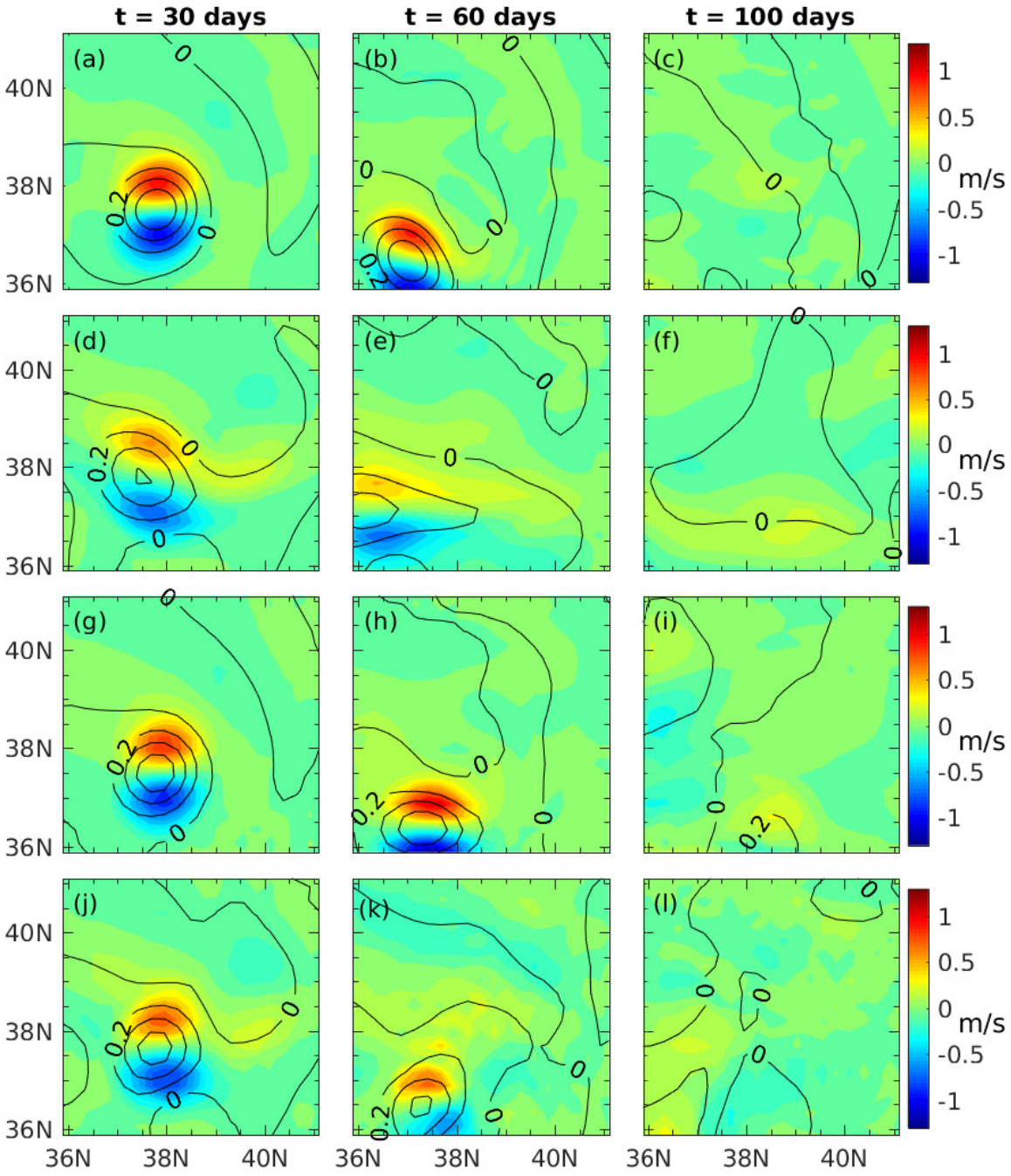

Fig. 6—SSU (shade) in the area covered by the nest as the baroclinic vortex evolves: (a-c) the high-resolution reference solution; the solution on the CM in (d-f) the 1-way nesting, (g-i) the full 2-way nesting, and (j-l) the simplified 2-way nesting. Superimposed are the contour lines of the CM SSH. The contour interval is 0.2 m.

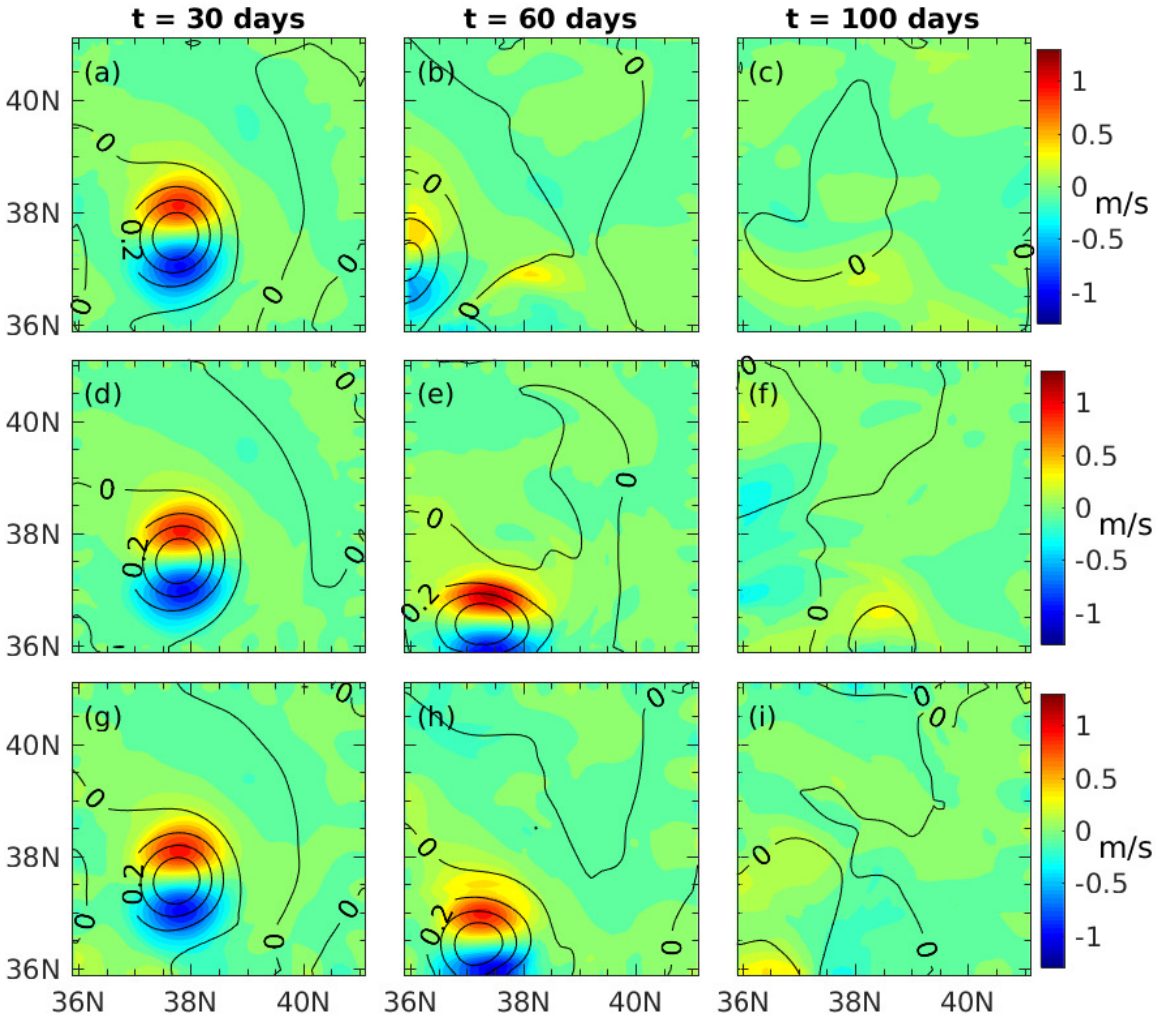

Fig. 7—SSU (shade) on the FM in (a-c) the 1-way nesting, (d-f) the full 2-way nesting, and (g-i) the simplified 2-way nesting. Superimposed are the contour lines of the FM SSH. The contour interval is 0.2 m.

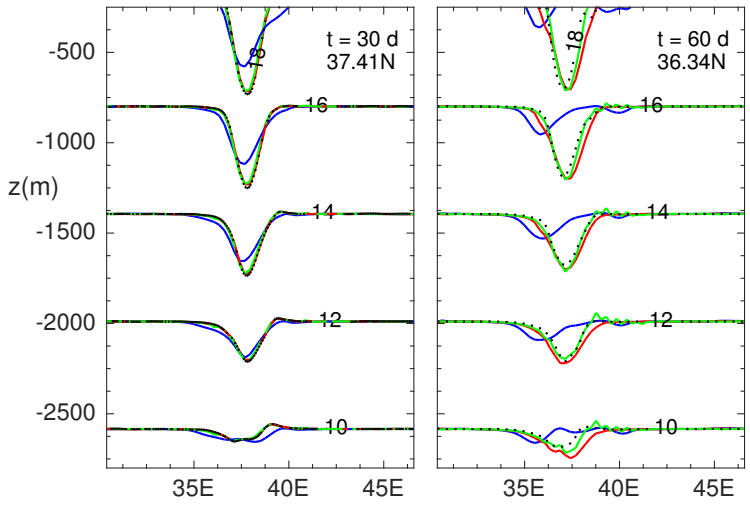

Fig. 8—Contours of the CM $T(^{\circ}\mathrm{C})$ in the (x,z) plane at the latitude passing through the vortex center (which is determined based on the SST of the high-resolution reference solution at the given time): the high-resolution reference solution (dotted black); the 1-way nesting (blue); the full 2-way nesting (red); the simplified 2-way nesting (green).

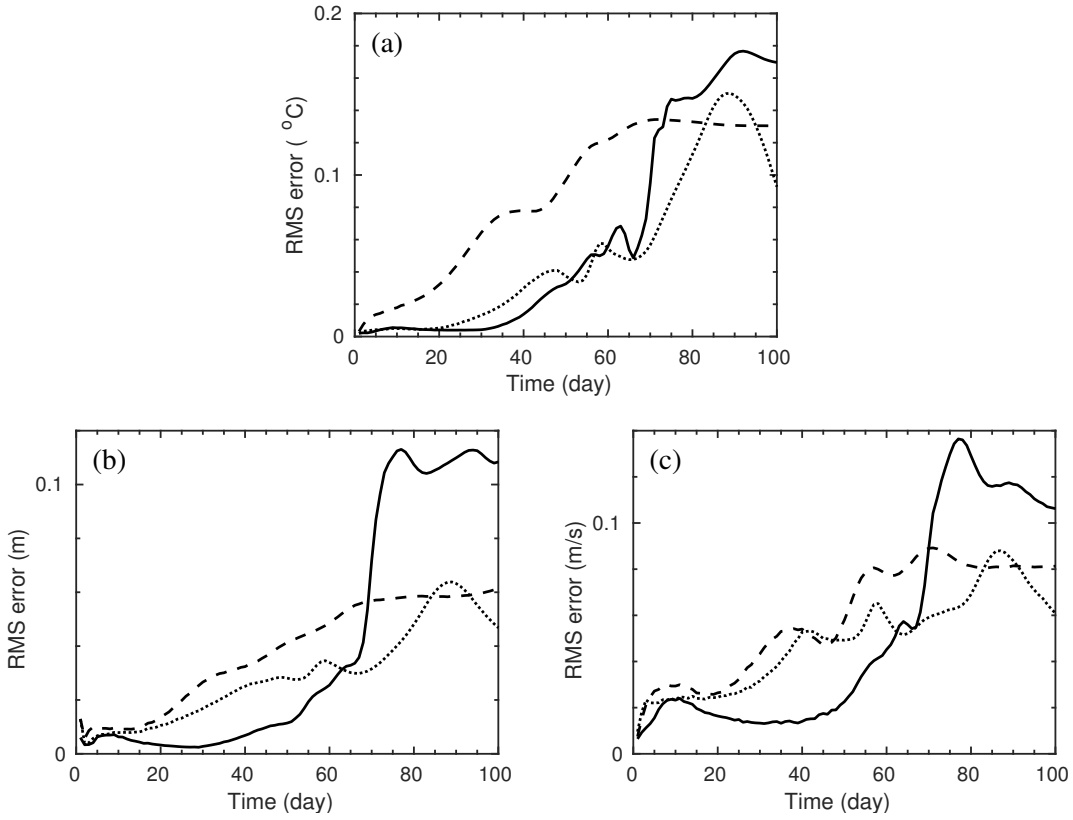

Fig. 9—RMS errors of (a) the CM SST, (b) the CM SSH, and (c) the CM SSU as functions of time. The curves are for the 1-way nesting (dashed), the full 2-way nesting (solid), and the simplified 2-way nesting (dotted).

5. APPLICATIONS ON REAL COASTS

5.1 Mississippi River delta

The non-nested NCOM is well tested in the Gulf of Mexico, since NRL has been running a 1-km resolution simulation in the region with COAMPS using 3D-var data assimilation with observations provided by NAVOCEANO, and archived the results from 2012 to the present date. For testing the embedded 2-way nesting procedure, we set up the parent grid with 3-km mesh size within the Gulf of Mexico, and a nest with 1-km mesh size in the Mississippi (MS) River Delta (Fig. 10). In this test, we use 40 vertical layers with the layer thickness increasing log-linearly downward. The top 20 are sigma-layers. The transition to z-layers is at about 140-m depth. The surface atmospheric forcing uses the NAVGEM05 database (3-hourly fields with a spatial resolution of 0.5°). The input data files for the boundary conditions are set up by interpolating the archived global HYCOM data (3-hourly fields with a spatial resolution of $1/12$ degree). Tides are specified using the Oregon State University US East Coast database (Egbert, Bennett and Foreman, 1994; Egbert and Erofeeva, 2002). The simulation period is from October 21, 2015 to April 16, 2016. The model results are output every 3 hours.

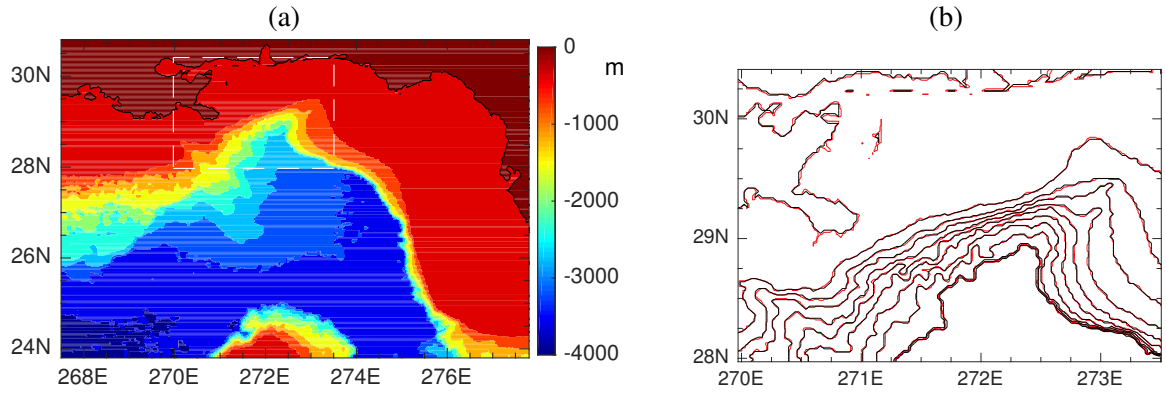

Fig. 10—(a) The model domain of the parent grid, with the dashed box indicating the nested area in the MS River Delta. The color shade shows the depth. (b) The depth contours in the nested area, showing the difference in the FM (red) and CM (black) bathymetry.

We have examined all of the model variables at different depths, and times. They are similarly informing, as far as evaluating the performance of 2-way nesting is of concern. Some examples are given below to facilitate the discussion.

The daily-averaged meridional sea surface current SSV and sea surface height SSH from the different nested simulations are shown in Fig. 11 and compared with the non-nested, 1-km simulation (i.e., the high-resolution reference solution). While the large-scale flow structures are similar overall, some differences are worth noting. (i) A trace of strong northward SSV (~ 0.5 m/s) that is associated with the low-salinity plume from the river mouth (at 29°09′04″N 89°12′27″W) is observed in both the 1-km reference solution and the full 2-way nesting (Figs 11a and 11c). This northward SSV at the river mouth, however, is practically absent on the CM in the 1-way nesting (Fig. 11b). Recall that the CM solution in the 1-way nesting is also the 3-km reference solution. (ii) The center of the anticyclonic eddy (e.g., the 0.8-m contour of SSH) is similarly located in the 1-km reference solution and in the full 2-way nesting. In the latter case, the eddy center is slightly further north, and the positive SSH contours extend further west, causing an enhanced northward current near 268E. On the CM in the 1-way nesting, the center of the anticyclonic eddy has a

lower pressure, and is closer to the river mouth (with the eddy center being further north by approximately 0.75° and slightly west of that in the 1-km reference solution). (iii) In the simplified 2-way nesting, the eddy has a smaller east-west range, and is closer to the river mouth than that in the 1-km reference solution and in the full 2-way nesting. (iv) The effects of lacking the appropriate grid-coupling are much more pronounced at small scales. For instance, the vertical velocity w on the CM is noisy in the nested area in the simplified 2-way nesting, and clearly discontinuous at the nest boundary (Fig. 12d). This is the consequence of not feeding the FM velocity fields back to the CM, despite the apparent smoothness of the large-scale fields in Fig. 11d. By comparison, the w-field in the full 2-way nesting is smooth on the CM, and the scale of the variations is visibly refined within the nested area (compare Fig. 12c with Fig. 12a and Fig. 12b); the nest boundary is barely visible. We note the noise at the south boundary ($\sim$ 24N) of the parent grid where the loop current of the Gulf Stream comes in. The boundary forcing for the parent grid is interpolated from the archived HYCOM database, which has a spatial resolution of $\sim$ 9 km. The parent grid is, in effect, a nest of the global ocean. The stronger noise in the 1-km reference solution is expected because of the greater contrast between the mesh sizes for the model domain and the database. While the noise at the boundary of the parent grid is inevitable (without advanced numerical treatments, e.g., sponge layers) due to the non-embedded (i.e., offline) nesting with the global (or another larger) domain, and undesirable, it in fact provides evidence to support the finding that the fully-coupled two-way grid-interaction tends to suppress the noise-generation at the nest boundary, in view of Fig. 12c. This is because the solutions on different grids become more consistent in the fully-coupled 2-way nesting, as is discussed below.

From the monthly sea surface salinity SSS, e.g., in March 2016 (Fig. 13 and Fig. 14), it is seen that the region of wind-induced freshwater mixing in the MS River Delta is consistently predicted on the CM and the FM in the full 2-way nesting (compare Fig. 14c and Fig. 14d), and is similar to that in the 1-km reference solution. In the 1-way nesting, however, this region of freshwater mixing is noticeably smaller on the CM than on the FM (compare Fig. 14a and Fig. 14b), with the latter being similar to the 1-km reference solution, as expected. This is consistent with the finding in the idealized experiments (Section 4) that the discrepancy between the CM and FM solution is greater in the 1-way nesting due to the lack of grid-coupling. In the simplified 2-way nesting, the monthly SSS on the CM and the FM appear to be consistent, and both compare well with the 1-km reference solution, but the CM velocity field is not satisfactory as we have seen in Fig. 12d.

The vertical profiles of temperature at a point just outside the river mouth are shown in Fig. 15, illustrating the fluctuations of the thermocline from March 22 to 27, 2016 in different simulations. On the CM in the full 2-way nesting, the upper layers are less warm, and the depth of the thermocline is shallower (by approximately 30 m), compared with the 1-km reference solution and the other nested simulations. However, it reveals a thermally inverted 21°C layer trapped in the 20-70 m depth range (Fig. 15c). In the full 2-way nesting, a cooler surface layer develops from 03/22 to mid 03/23, which reappears on 03/25 with an even lower temperature. These events are similarly seen in the 1-km reference solution, though only a slightly cooler surface layer reappears on 03/26. These events are not visible on the CM in the simplified 2-way nesting or in the 1-way nesting. The field observations of the vertical temperature profiles at this point are shown in Fig. 16a for the same time period. (The dataset is from the field experiment of OL16 (Optical Layers, March 2016), which was a joint study of NRL, Harbor Branch Oceanographic Institute, and the University of North Carolina. The data were collected from an ADCP mooring array. Note that a comprehensive comparison with the field experiment, including other datasets, is beyond the scope of this paper.) The observed upper layers are somewhat cooler and thicker than the simulated results, including the 1-km reference solution. It is, however, interesting to note that a better comparison with the data is given by the full 2-way nesting, including the thermally inverted 21°C layer (though it occurs at deeper depths in

the data). Furthermore, the formation of a cooler surface layer is also seen in the data from 03/22 to 03/23, and around 03/26. For a closer look, we compare the vertical temperature profiles on 03/22/2016 at 15:00 GMT in Fig. 16b. The full 2-way nesting is seen to closely follow the data in the upper layers ($z > -60$ m), but under-estimate the data in the lower layers. All the other simulations over-estimate the data in the upper layers, but compare well with the data for $z < -70$ m. The thermal inversion is absent from the 1-km reference solution, and nearly so in the CM solution of the 1-way nesting. In the simplified 2-way nesting, a thermally inverted layer of higher temperature occurs.

In the 1-way nesting, there is a considerable discrepancy between the temperature profiles on the CM and FM in the upper depth that extends well below the thermocline (Fig. 17). This inconsistency is clearly corrected by feeding back the FM fields. (This, however, does not explain why the 1-km reference solution over-predicts the data in the upper layers, while T_{CM} in the full 2-way nesting agrees better with the data.)

Mobile Bay is another area of major practical interest, and can be strongly affected by the northeastward low-salinity plume from the MS River. As an example, we show the fluctuation of T at a point just outside Mobile Bay (Fig. 18a) in March 2016. On the CM, the results from the nested simulations are generally similar, and follow the 1-km reference solution. Note the sudden drop of temperature around 03/21 and the subsequent recovery following 03/23, which coincide with the events of retreat and reformation of the freshwater plume from the MS River. Again, the 1-way nesting gives the largest difference between the solutions on the CM and the FM (Fig. 18b).

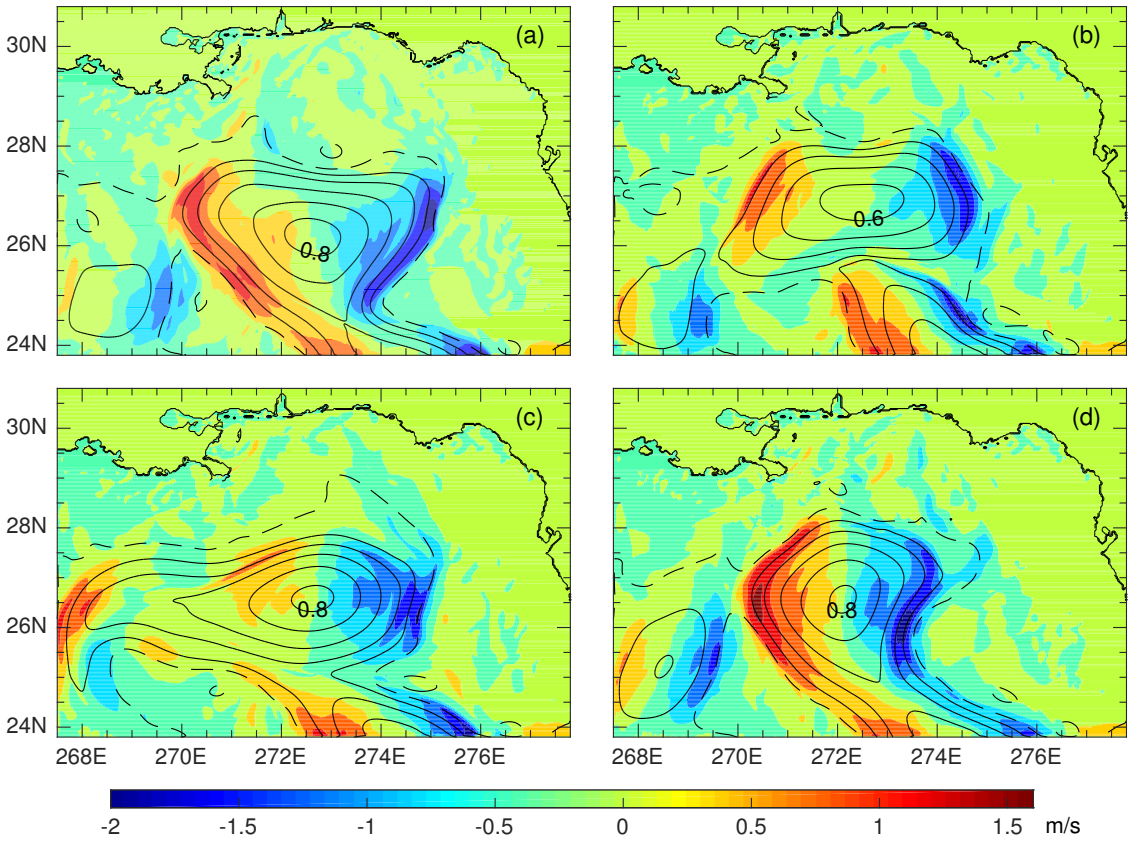

Fig. 11—Daily-averaged meridional sea surface current SSV (shade) on March 19, 2016, superimposed by the contours of SSH, showing the anticyclonic eddy that is nearly breaking off from the loop current (below 24N): (a) the 1-km reference solution; (b) the 1-way nesting; (c) the full 2-way nesting; (d) the simplified 2-way nesting. The contour interval is 0.2 m, with the dashed lines for the negative values.

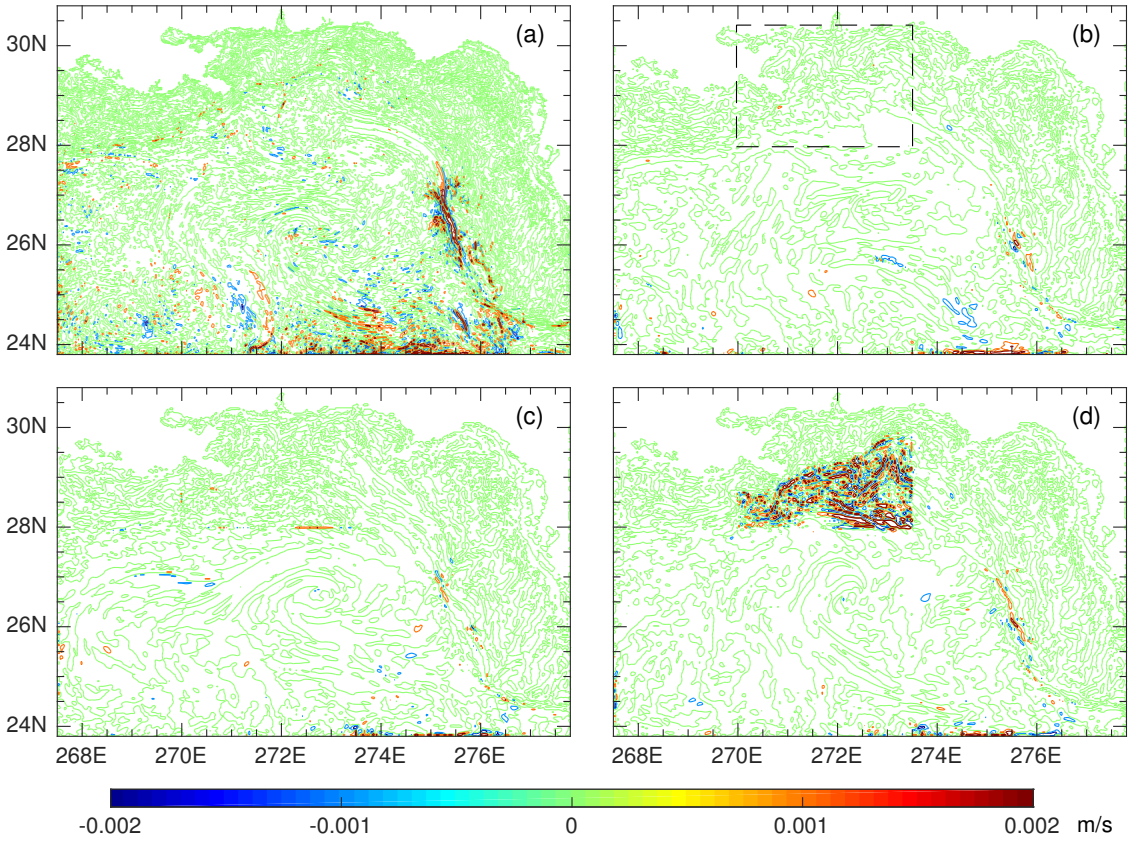

Fig. 12—Vertical velocity w at $z = -94.05$ m (layer 18) on March 19, 2016, 12:00 GMT: (a) the 1-km reference solution; the CM solution in (b) the 1-way nesting (also the 3-km reference solution), (c) the full 2-way nesting, and (d) the simplified 2-way nesting. The dashed box in (b) indicates the nested area.

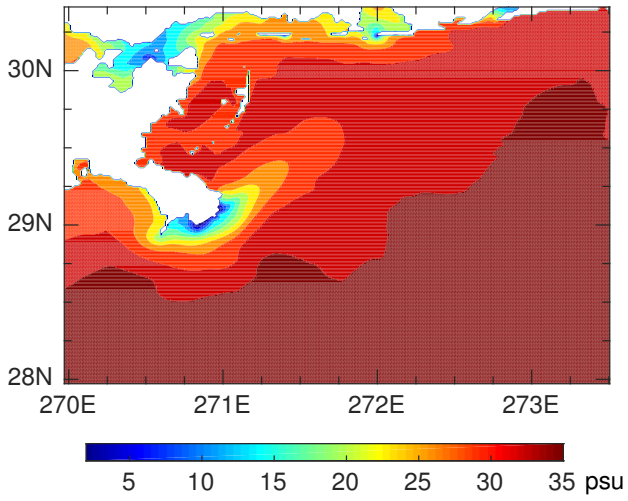

Fig. 13—The 1-km reference solution of the monthly SSS in March 2016, showing the wind-induced freshwater mixing in the MS River Delta. Only the area that would be covered by the nest is shown.

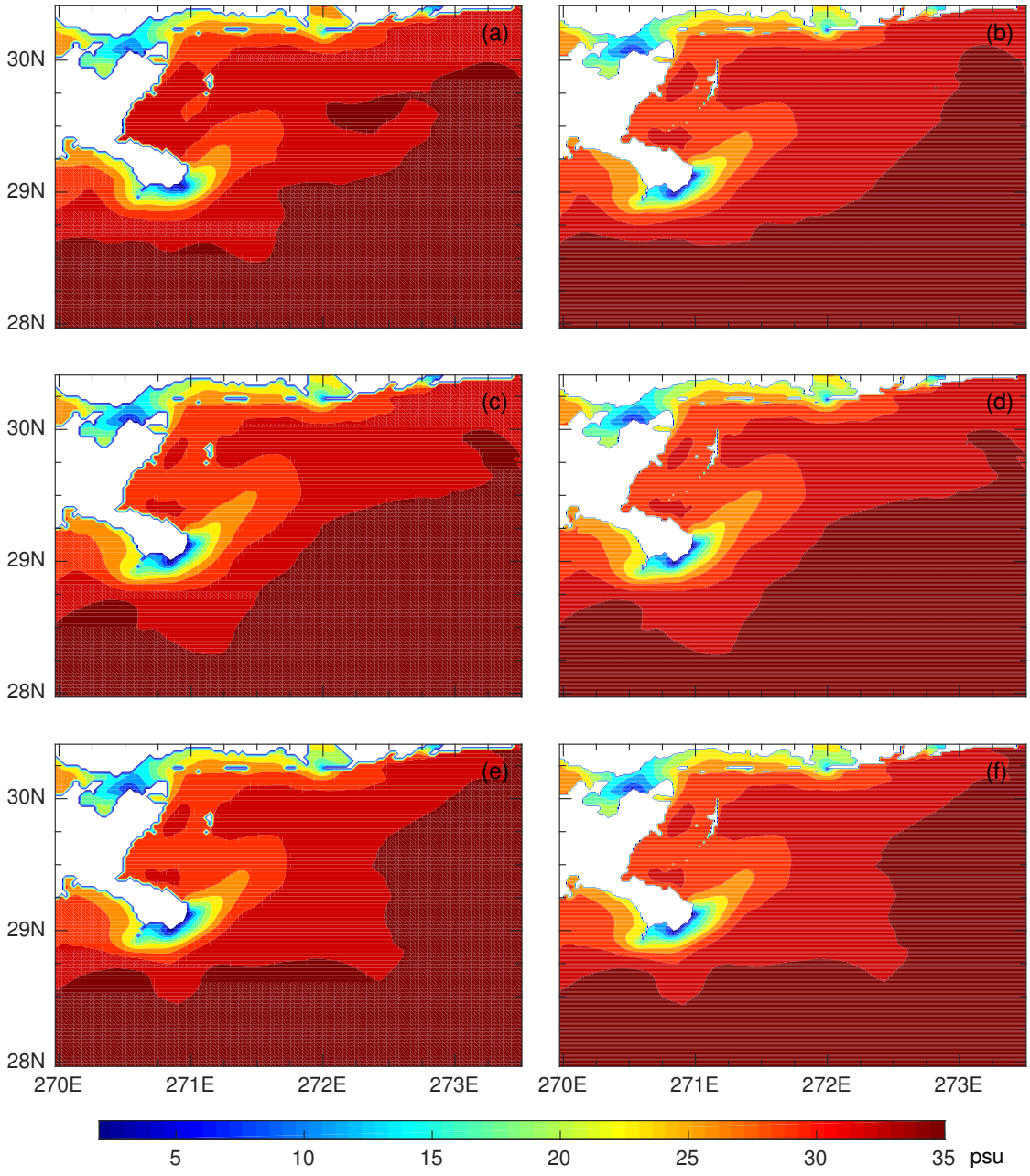

Fig. 14—Monthly SSS in March 2016 from the nested simulations, comparing the solutions in the nested area on the CM (left panels) with the FM solutions on the nest (right panels): (a-b) the 1-way nesting; (c-d) the full 2-way nesting; (e-f) the simplified 2-way nesting.

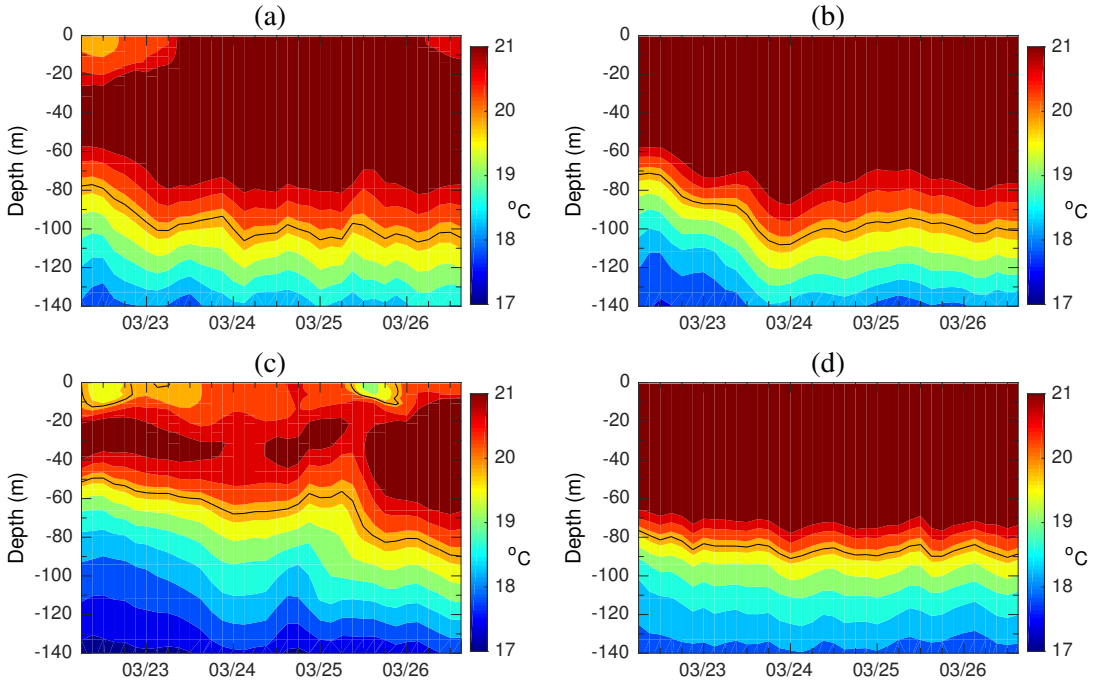

Fig. 15—Temperature variations in depth-time at a point (271.4427E, 28.9795N) just outside the MS River mouth: (a) the 1-km reference solution; the CM solution in (b) the 1-way nesting, (c) the full 2-way nesting, and (d) the simplified 2-way nesting. The 20°C contour is marked in black.

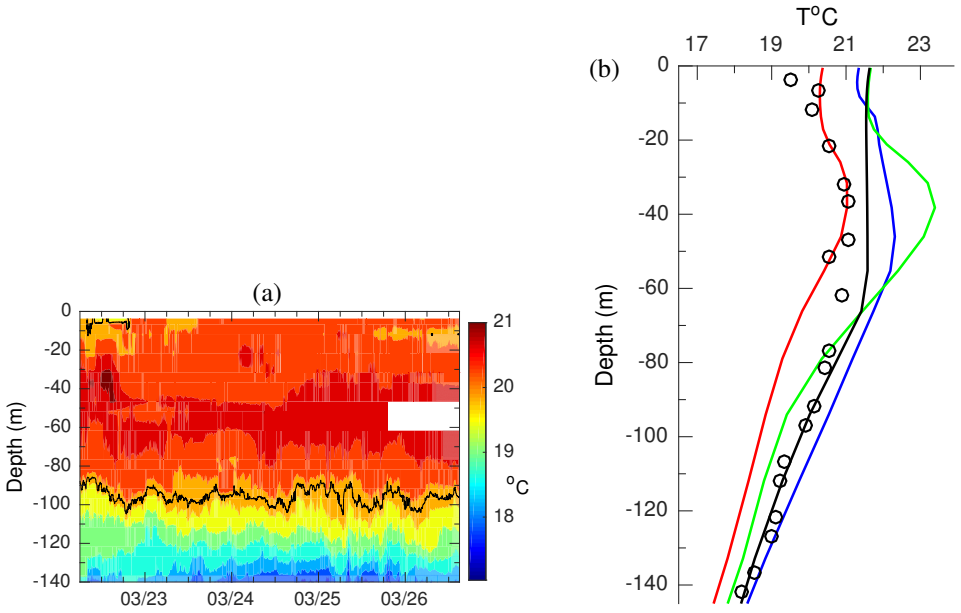

Fig. 16—(a) Temperature profiles at (271.4427E, 28.9795N) from the OL16 field experiment. Data were collected at 19 depths from $z = -141.7$ to -3.7 m at 1 min intervals from 03/22/2016 06:00 to 03/26/2016 16:59 GMT. The data gap (white) at the end of the time series is due to the failure of a sensor. (b) Depth variation of T at 15:00 GMT on 03/22/2016. Data: ∘. Curves: the 1-km reference solution (black); the 1-way nesting (blue); the full 2-way nesting (red); the simplified 2-way nesting (green).

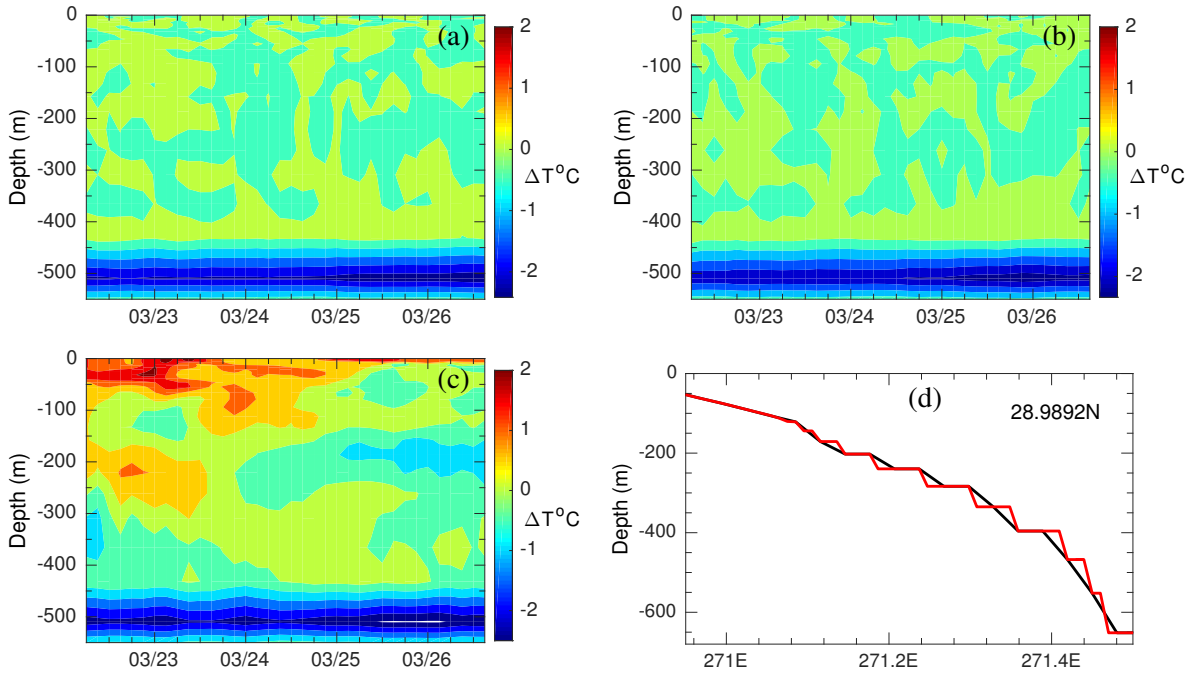

Fig. 17—Differences of temperature profiles on the CM and the FM, $\Delta T = T_{\rm CM} - T_{\rm FM}$, at (271.4427E, 28.9795N): (a) the full 2-way nesting; (b) the simplified 2-way nesting; (c) the 1-way nesting. In (d), the depths near 271E on the CM (black) and the FM (red) are shown. Note that there is no bathymetry discrepancy in the sigma layers ($z > -120$ m).

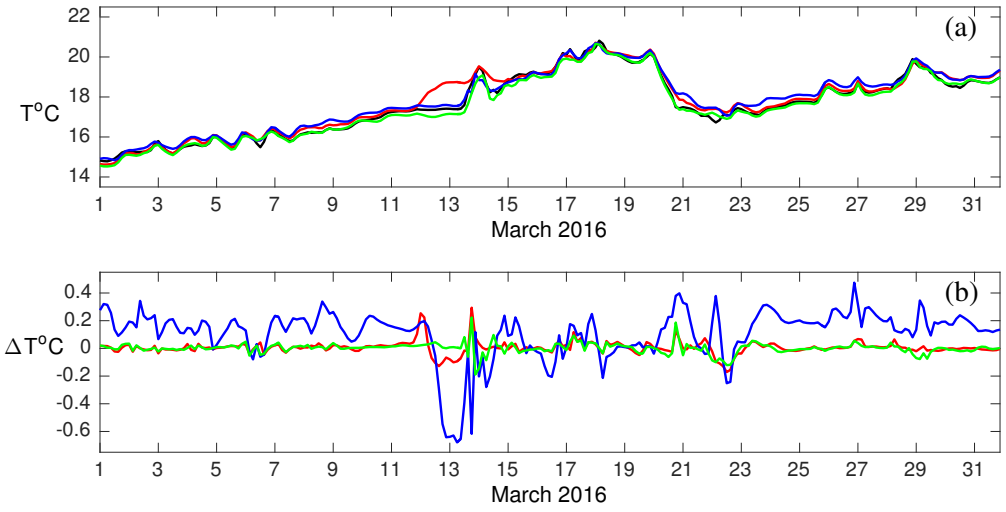

Fig. 18—(a) Temperature fluctuations at a point (271.87542E, 30.12943N, and 12-m depth) just outside Mobile Bay: the 1-km reference solution (black); the solution on the CM in (red) the full 2-way nesting, (green) the simplified 2-way nesting, and (blue) the 1-way nesting. (b) $\Delta T = T_{\rm CM} - T_{\rm FM}$ at this point in (red) the full 2-way nesting, (green) the simplified 2-way nesting, and (blue) the 1-way nesting.

5.2 Columbia River on the Pacific northwest coast

This test case is for the Pacific northwest region where the Columbia River discharges into the ocean (Fig. 19). Again, we use a 3-km horizontal mesh for the parent grid and 40 vertical layers with the layer thickness increasing log-linearly downward. The top 20 layers are sigma coordinate. A FM nest is set up south of the Columbia River mouth (at 46.3N 124.0W) and downstream of the fresher-water plume. The surface atmospheric forcing is set up using the NOGAPS database (3-hourly fields with a spatial resolution of 0.5°). The boundary conditions are set up by interpolating the archived Global NCOM data (6-hourly fields with a spatial resolution of 10 km). Tides are specified using the Oregon State University US West Coast database. The simulation period is 90 days, from 2012040100 to 2012063000.

The results from the nested simulations (the 1-way nesting, the full and simplified 2-way nesting) and the 1-km non-nested simulation are compared in Figs. 19 – 26. In the simplified 2-way nesting, the CFL condition for the vertical advection slightly exceeded 1.0 on the CM during the 90-day simulation, and could not be reduced by changing the numerical open boundary condition options for the nest; the high production of noise affects the large-scale horizontal velocity fields on the CM even at the early stages of the simulation (e.g., the SSV in Fig. 21d). In the full 2-way nesting, the large-scale fields are smooth on the CM, showing no trace of the nest (which is only slightly visible in the vertical velocity field in Fig. 23c). This again shows that the two-way nesting procedures are adequate to facilitate smooth interactions between the grids. This is, however, insufficient to conclude that the full 2-way nesting has improved the solutions on the parent grid during the 90-day simulation, in view of the overall similar large-scale structures of the fields from the 1-km and 3-km reference solutions, and the results from the full 2-way nesting.

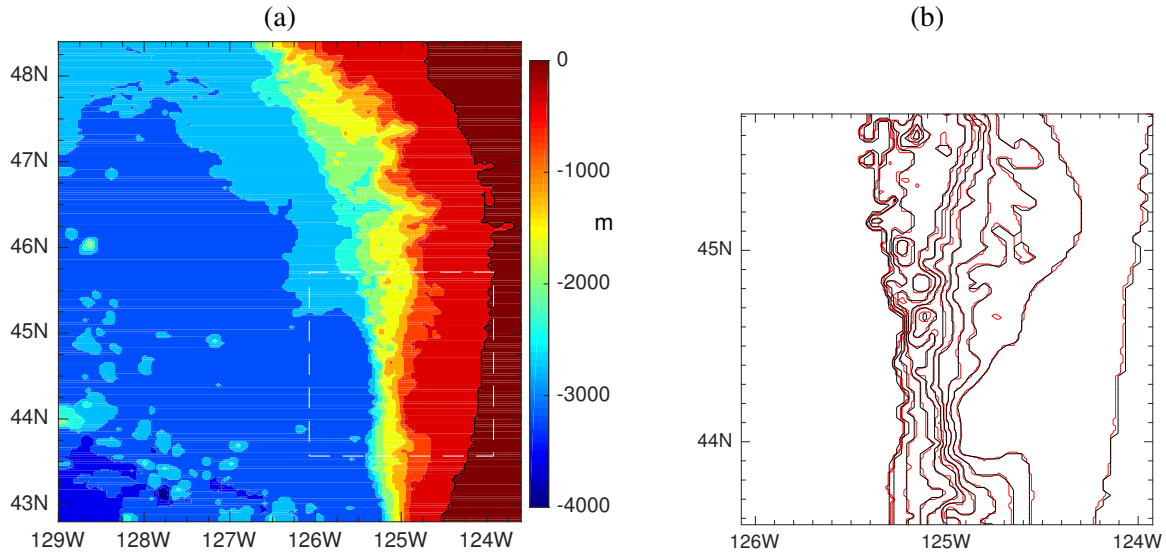

Fig. 19—(a) The modeling domain of the parent grid (CM) for simulating the Columbia River on the North Pacific coast, with the dashed box showing the nest (FM). The color shade shows the depth. (b) The depth contours in the nested area, showing the difference in the FM (red) and CM (black) bathymetry.

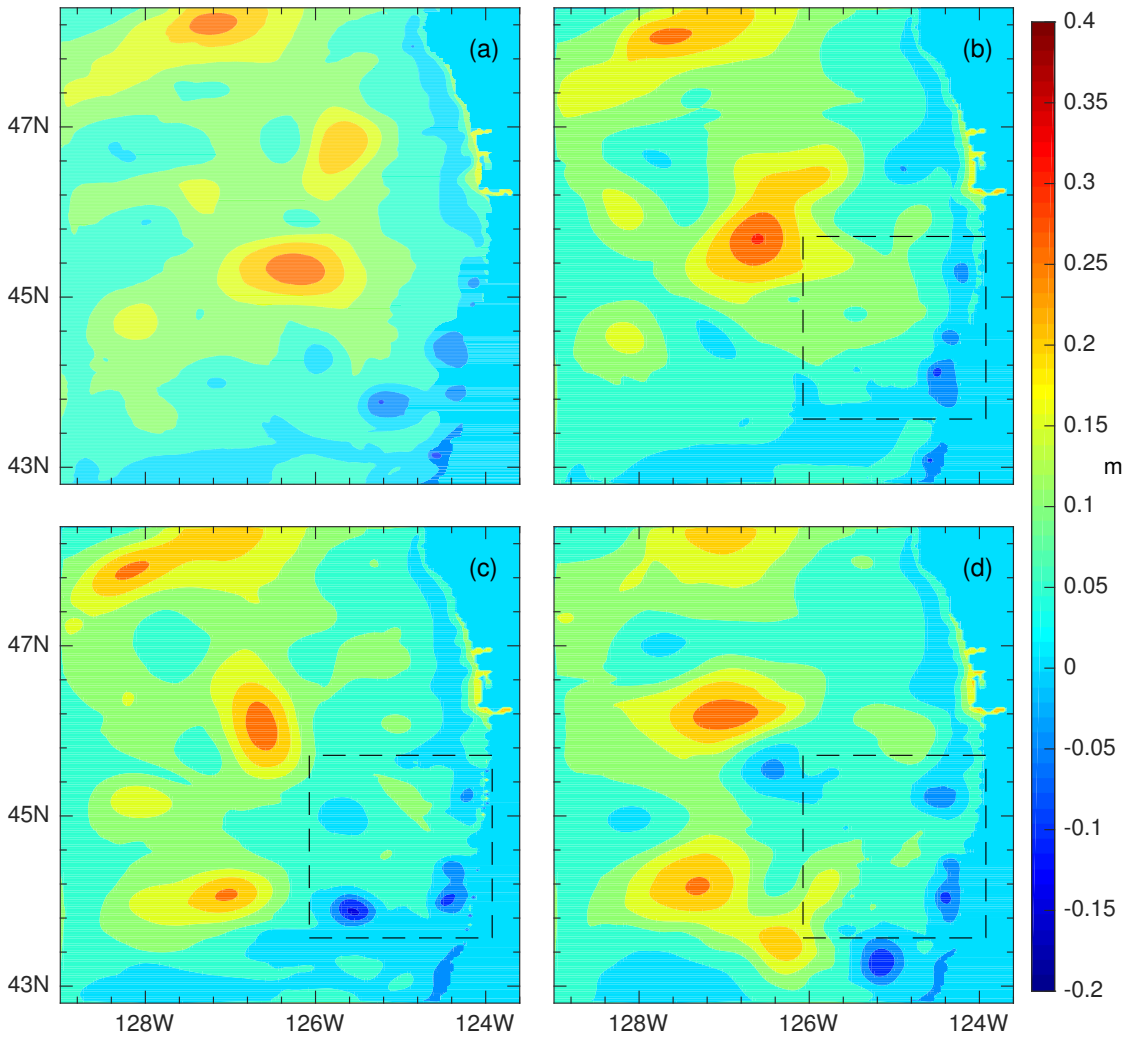

Fig. 20—SSH on day 90 (06/29/2012, 00:00GMT) of the Columbia River simulations: (a) the 1-km reference solution; (b) the 1-way nesting (also the 3-km reference solution); (c) the full 2-way nesting; (d) the simplified 2-way nesting. The dashed box indicates the nested area.

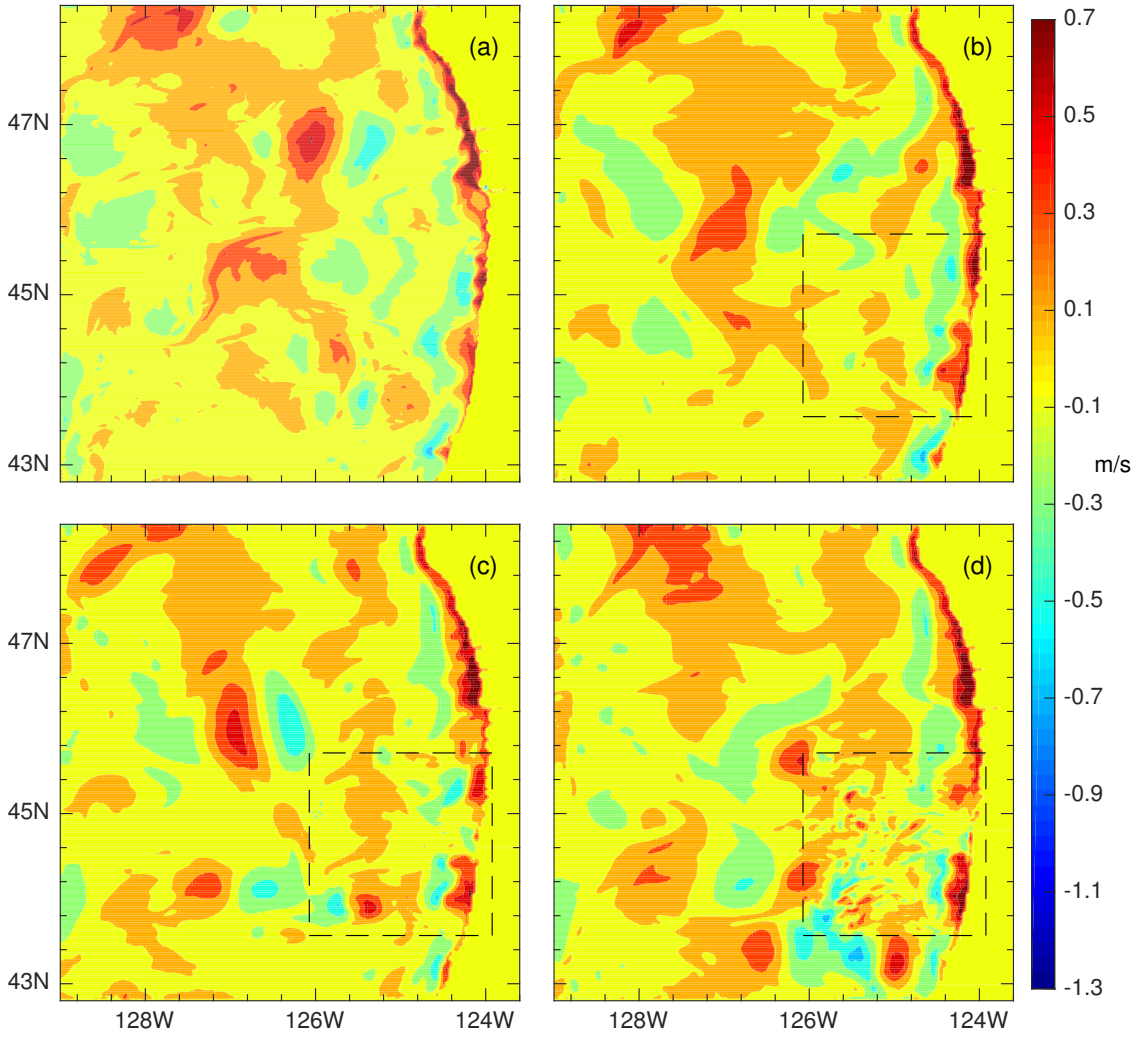

Fig. 21—Meridional sea surface current SSV on day 90 (06/29/2012, 00:00GMT): (a) the 1-km reference solution; (b) the 1-way nesting; (c) the full 2-way nesting; (d) the simplified 2-way nesting.

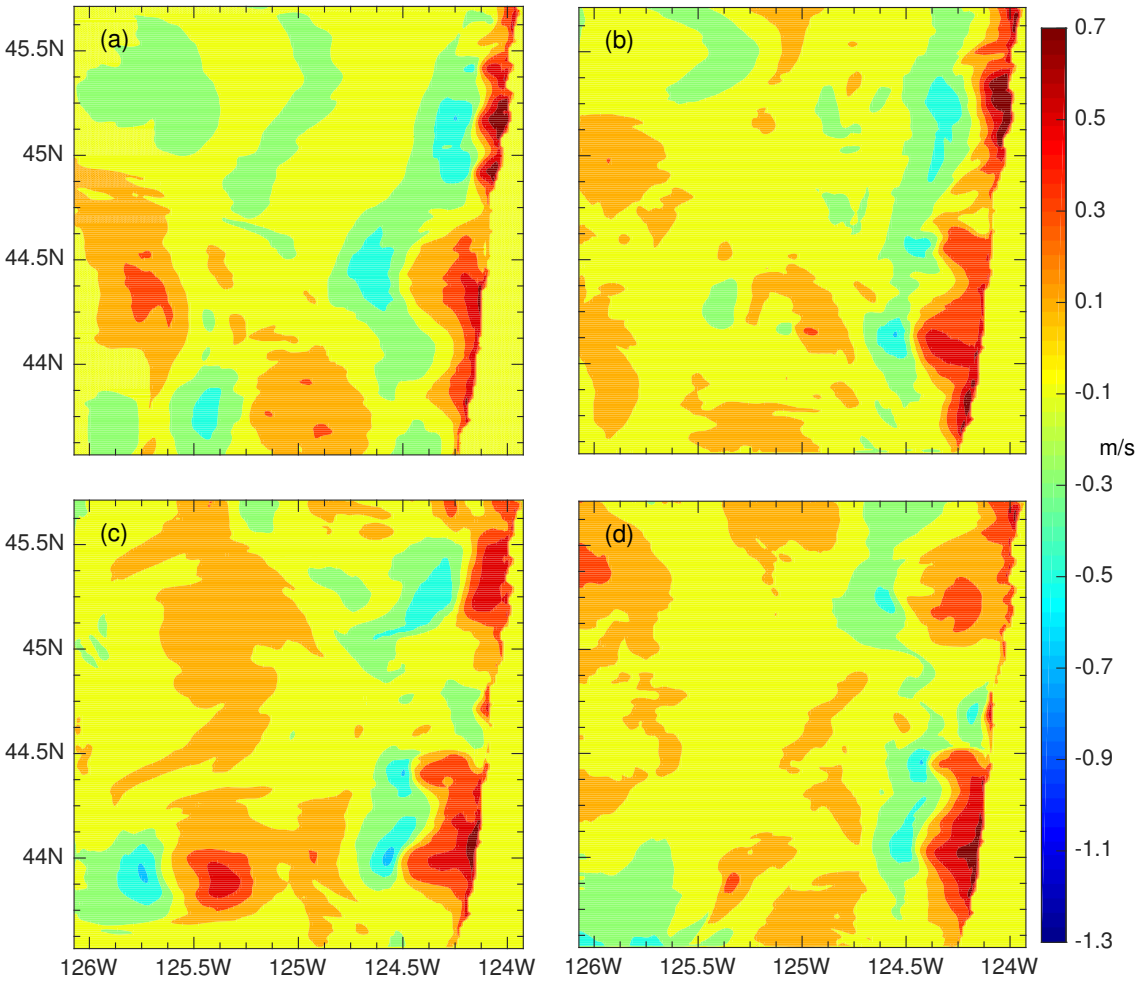

Fig. 22—FM SSV on day 90 (06/29/2012, 00:00GMT): (a) the 1-km reference solution in the nested area; solutions on the nest in (b) the 1-way nesting, (c) the full 2-way nesting, and (d) the simplified 2-way nesting. Note the absence of noise in the FM field in (d), compared with the noisy field in the nested area on the CM in Fig. 21d (which is the consequence of not feeding back the FM velocity fields).

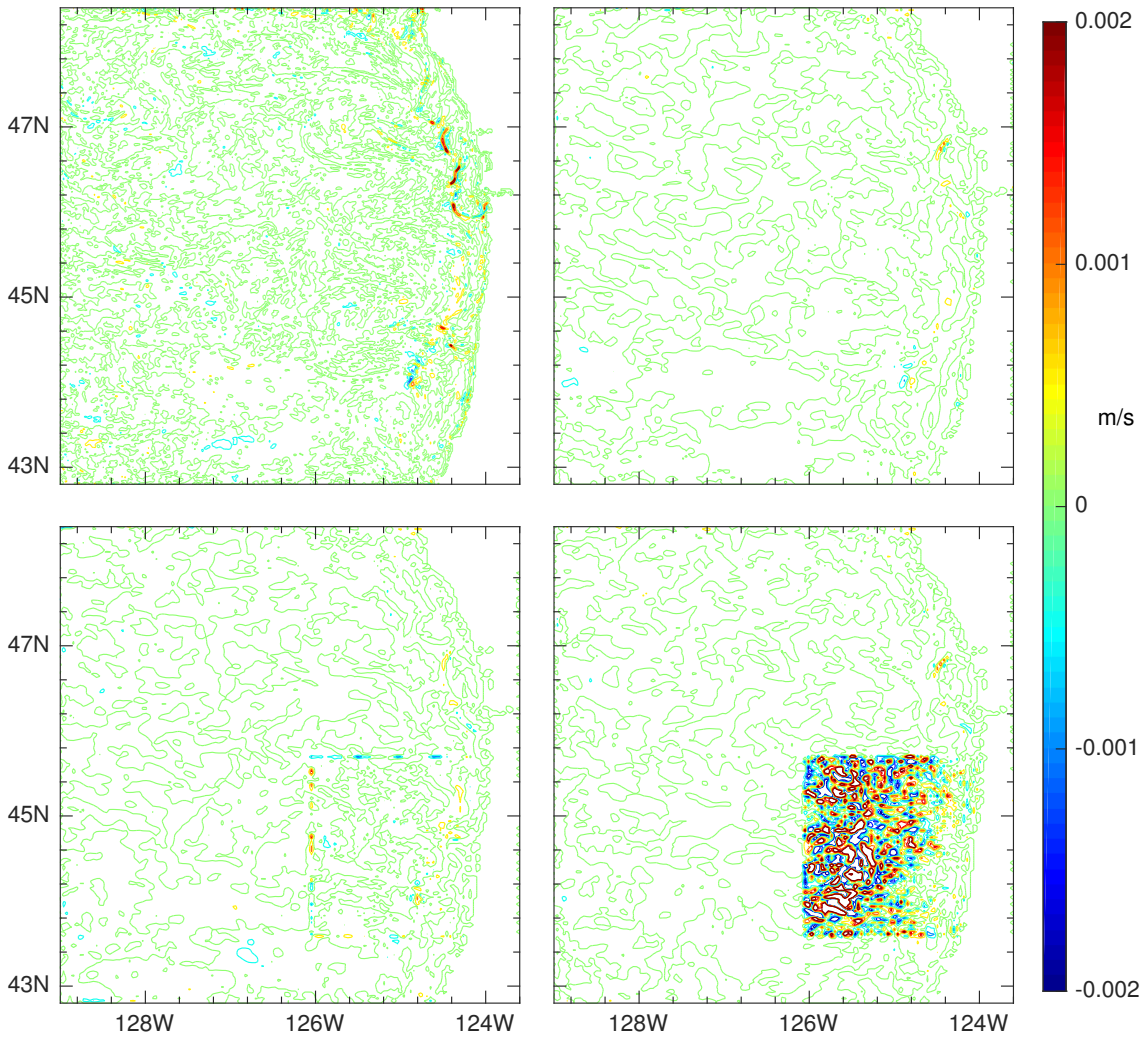

Fig. 23—Vertical velocity w at $z = -94.05$ m (layer 18) on 05/01/2012, 00:00GMT: (a) the 1-km reference solution; (b) the 1-way nesting (also the 3-km reference solution); (c) the full 2-way nesting; (d) the simplified 2-way nesting.

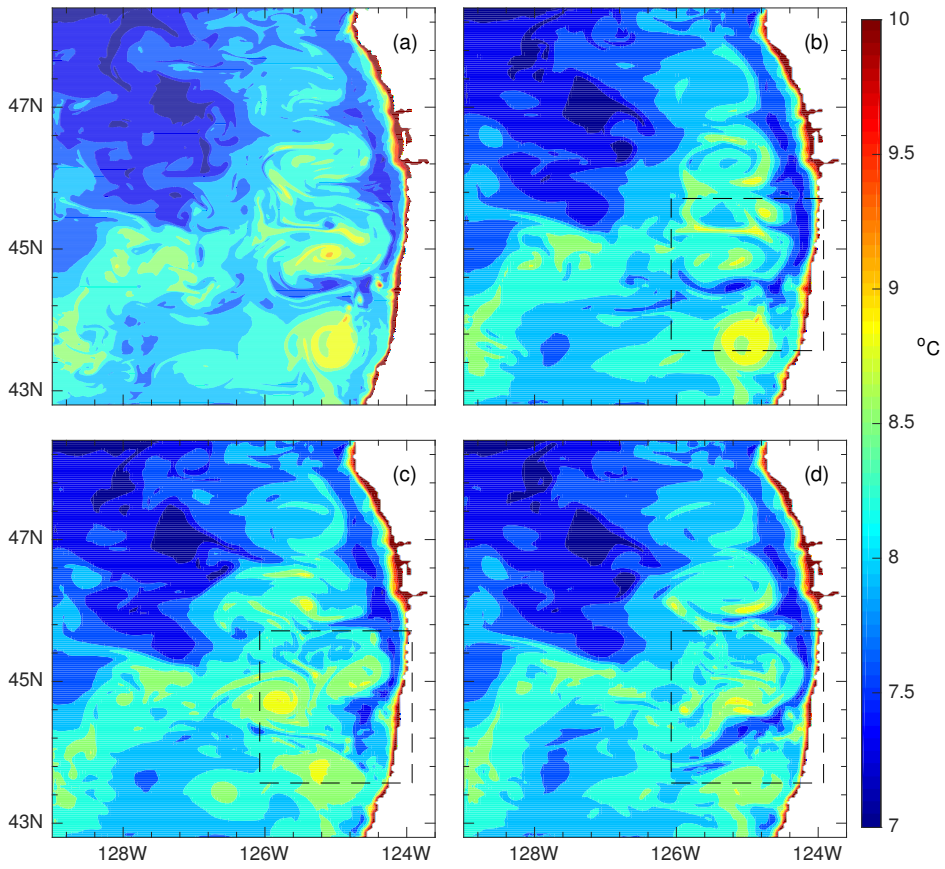

Fig. 24—Temperature at $z = -94.05$ m (layer 18) on 05/01/2012, 00:00GMT: (a) the 1-km reference solution; (b) the 1-way nesting; (c) the full 2-way nesting; (d) the simplified 2-way nesting.

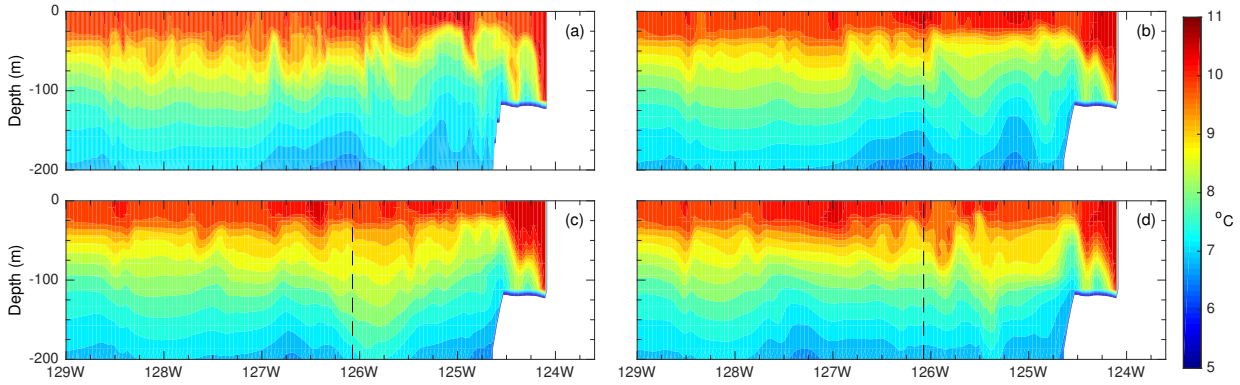

Fig. 25—Temperature variation in depth on the CM at 44.5N on 05/01/2012, 00:00GMT: (a) the 1-km reference solution; (b) the 1-way nesting; (c) the full 2-way nesting; (d) the simplified 2-way nesting. The dashed vertical line is the seaward boundary of the nest.

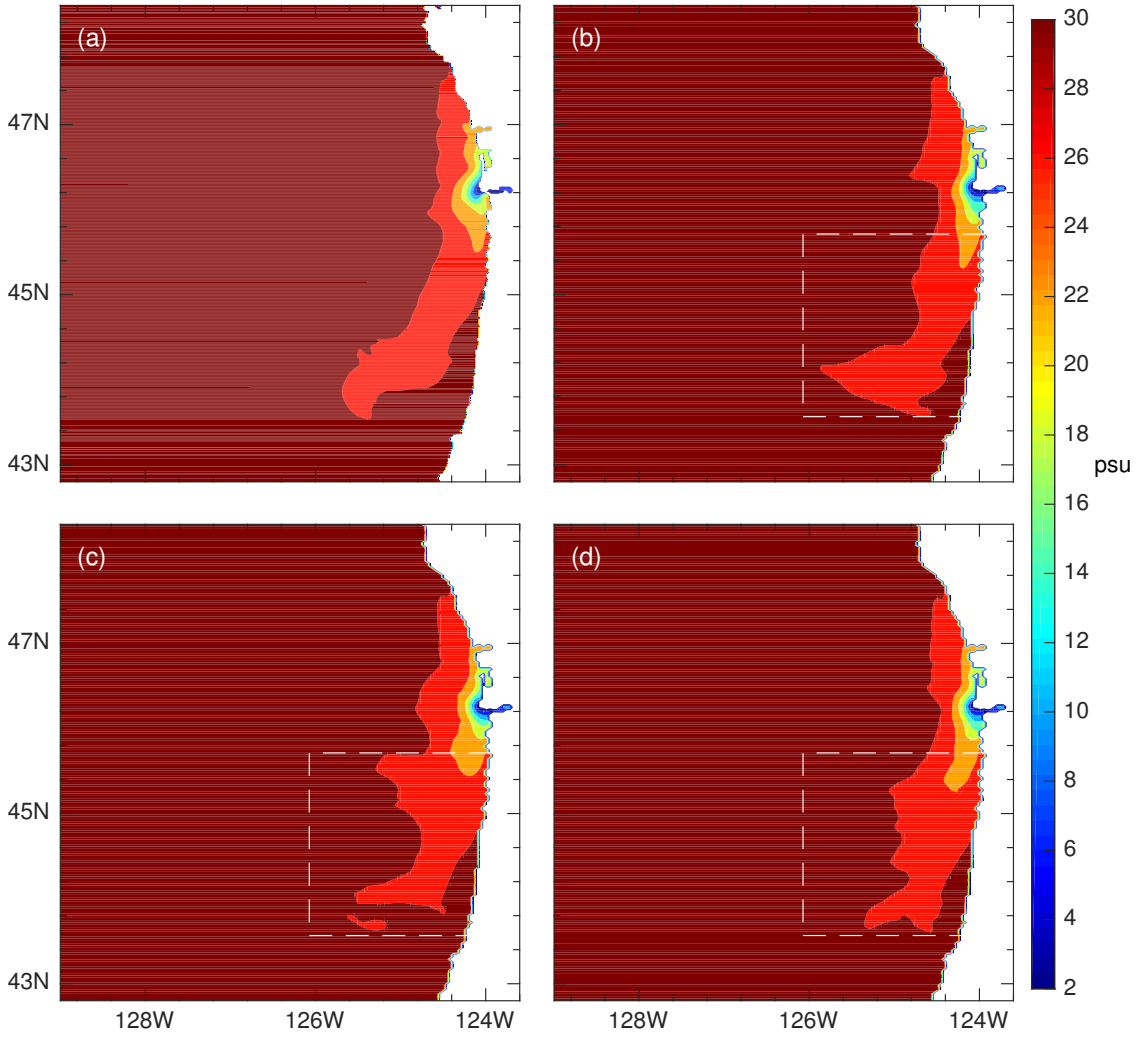

Fig. 26—Monthly SSS in 06/2012: (a) the 1-km reference solution; (b) the 1-way nesting; (c) the full 2-way nesting; (d) the simplified 2-way nesting.

6. SUMMARY

We have given a detailed documentation of the implementation and testing of embedded nesting in NCOM. In the previous development of 1-way nesting in NCOM, we have implemented and validated the interpolation schemes to obtain the boundary conditions/forcing for the fine-mesh (FM) nests from the coarse-mesh (CM) fields on the parent grid. Thus, the attention here is on the strategies of feeding back the fields from the FM to the CM in the 2-way nesting.

The feedback procedure in NCOM includes: (a) the appropriate separation of the dynamic interfaces (where the FM boundary conditions are calculated) and the feedback interfaces (which set the outer limits of feeding back the FM fields); (b) the feedback (averaging) operators for the scalars and velocity fields; (c) the correction of the 3D baroclinic velocities to match the depth-integrated barotropic transports in the feedback. The inconsistency between the baroclinic velocities and the barotropic transports is inherently due to the presence of bathymetry, and cannot be overcome by making the bathymetry consistent, or even identical, on the child and parent grids. Not to mention that the discrepancies in bathymetry are virtually unavoidable in practical applications because of the grid resolutions. The remedy used for (c) is simple, but effective, and proven to be necessary in realistic coastal simulations to avoid CFL violations on the CM. In NCOM's setup programs, an option is provided to update the CM depths after setting up the nests, which tends to improve the bathymetry consistency.

The implementations of the 2-way nesting are tested using idealized experiments and simulations on real coasts, and evaluated by comparing the results from the 1-way nesting, the full and simplified 2-way nesting, and the high-resolution, non-nested simulations (i.e., the reference). The simplified approach feeds back only the temperature and salinity from the FM to the CM, assuming that the CM velocity fields will be indirectly updated when the flow dynamics are dominantly in geostrophic balance. The full 2-way nesting is capable of smoothly fusing the FM and CM fields, leaving little indication of discontinuity/noise in the nested area in the CM horizontal fields; and the nest locations are only slightly visible in the vertical velocity field (which is of smaller scale) on the CM. In cases where the results are sensitive to the grid resolution (e.g., the evolution of a baroclinic vortex), the CM solution is markedly improved in the full 2-way nesting, becoming more consistent with the FM solution on the nest. The simulation of the Mississippi River Delta shows the improved prediction of features associated with the fresher-water plume on the CM due to the feedback of the FM fields, and is supported by the comparison with a field dataset (though this model-data comparison is limited in scope). While the simplified 2-way nesting can, to some extent, improve the consistency of solutions on the FM and CM when the geostrophic balance dominates, its skill is limited. The noise-production on the CM is strong in the simplified approach due to the lack of directly feeding back the FM velocity fields, making the nested area clearly visible in the vertical velocity field; in some cases (e.g., the Columbia River simulation on the Pacific northwest coast), the noise can be so strong that unrealistic fine structures become visible in the large-scale horizontal fields on the CM, and large, advective CFL violations occur. Thus, the full 2-way nesting is always recommended when two-way grid-coupling is needed.

ACKNOWLEDGMENTS

We thank Dr. Ann Rice for sharing the dataset from the field experiments of Optical Layers 2016. This work is part of the Naval Research Laboratory 6.2 program "River Influence at Multi-scales" funded by Office of Naval Research.

Appendix A

INITIAL CONDITIONS FOR THE BAROCLINIC VORTEX PROBLEM

The dynamic pressure that is used in Penven et al (2006) to initialize the baroclinic vortex motion has the form $P = P_0 F(z) \mathrm{e}^{-(x^2+y^2)/2\lambda^2}$, where the constant $P_0 = \rho_0 f_0 u_m \lambda \mathrm{e}^{1/2}$. The maximum surface geostrophic velocity $u_m = 1$ m/s, following Spall and Holland (1991). The horizontal e-folding scale $\lambda = 60$ km at the surface. The vertical distribution $F(z) \equiv 0$ for $z \leq -H_1$ so that there is no motion below the prescribed depth H_1, where the density field remains horizontally uniform. For $z > -H_1$, Penven et al. (2006) chose

$$F(z) = \frac{H_1 - 1 + z + \mathrm{e}^{-(z+H_1)}}{(H_1 - 1 + \mathrm{e}^{-H_1})}, \tag{A1}$$

which satisfies $F(z=0) = 1$ (so that the magnitude of the surface pressure distribution is controlled by P_0), and $F(z=-H_1) = F'(z=-H_1) = 0$. While the last two conditions ensure the continuity of F and its derivative F' at $z = -H_1$, F' is practically discontinuous as $z \to -H_1$ because of the rapid variation (Fig. A1). This affects the smoothness of the density field, since the density perturbation corresponding to the dynamics pressure is determined by $-\partial P/\partial z = -\tilde{\rho} g$, where g is the gravitational acceleration.

We choose a slightly different function of the vertical distribution for $z > -H_1$, i.e.,

$$f(z) = \left(\frac{z}{H_1} + \mathrm{e}^{-(1+z/H_1)} \right) \mathrm{e}, \tag{A2}$$

which also satisfies $f(z=0) = 1$, and $f(z=-H_1) = f'(z=-H_1) = 0$. The derivative $f'(z)$, however, is smooth for $z > -H_1$ (Fig. A1). For $z \leq -H_1$, $f(z) \equiv 0$. Other initial fields are then calculated, assuming the geostrophic balance for the horizontal velocities and hydrostatic balance in z accounting for the surface elevation, as in Penven et al. (2006). The temperature field is from $\rho = 1030 - 0.28T\,(^\circ\mathrm{C})$.

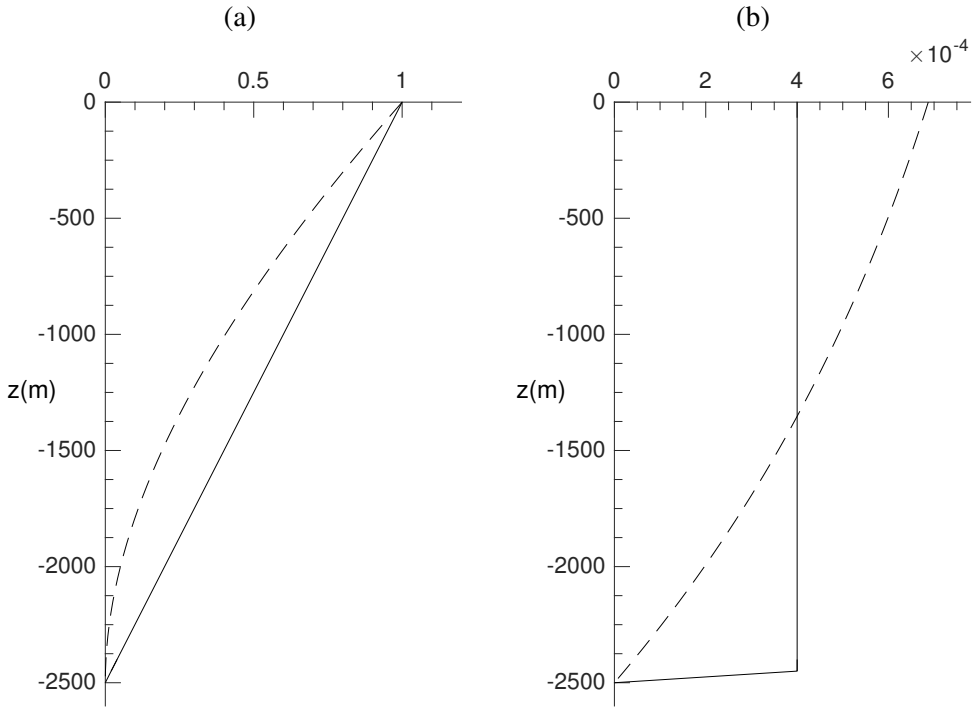

Fig. A1—(a) Functions: solid, $F(z)$; dashed, $f(z)$. (b) Derivatives: solid, $F'(z)$; dashed, $f'(z)$.

REFERENCES

1. Barron, C. N., Kara, A. B., Martin, P. J., Rhodes, R. C. & Smedstad, L. F. 2006 Formulation, implementation and examination of vertical coordinate choices in the Global Navy CoastalOcean Model (NCOM). *Ocean Modell.*, **11**, 347–375.

2. Debreu, L. & Blayo, E. 2008 Two-way embedding algorithms: a review. *Ocean Dyn.*, **58**, 415–428.

3. Debreu, L., Marchesiello, P., Penven, P. & Cambon, G. 2012 Two-way nesting in split-explicit ocean models: Algorithms, implementation and validation. *Ocean Modell.*, **49-50**, 1–21.

4. Egbert, G. D., Bennett, A. F. & Foreman, M. G. G. 1994 TOPEX/Poseidon tides estimated using a global inverse model. *J. Geophys. Res.*, **99**, 24821–24852.

5. Egbert, Gary D. & Svetlana Y. Erofeeva 2002 Efficient inverse modeling of barotropic ocean tides. *J. Atmos. Oceanic Technol.*, **19** (2), 183–204.

6. Haley, P. J. Jr. & Lermusiaux, P. F. J. 2010 Multiscale two-way embedding schemes for free-surface primitive equations in the "Multidisciplinary Simulation, Estimation and Assimilation System?. *Ocean Dyn.*, **60**, 1497–1537.

7. McWilliams, J. C. & Flierl, G. R. 1979 On the evolution of isolated, nonlinear vortices. *J. Phys. Oceanogr.*, **9** (6), 1155–1182.

8. Martin, P. J. 2000 Description of the Navy coastal ocean model version 1.0. NRL Report No. NRL/FR/7322-00-9962, 45 pp. (Available from NRL, Code 7322, Bldg. 1009, Stennis Space Center, MS 39529-5004,USA).

9. Martin, P. J., Edwards, K. L., Hebert, D. A. & Allard, R. A. 2015 Implementation of Wetting and Drying in NCOM: Description and Validation Test Report. NRL Report No. NRL/MR/7320-15-9573. 51 pp. (Available from NRL, Code 7322, Bldg. 1009, Stennis Space Center, MS 39529-5004,USA).

10. Penven, P., Debreu, L., Marchesiello, P. & McWilliams, J. C. 2006 Evaluation and application of the ROMS 1-way embedding procedure to the central California upwelling system. *Ocean Modell.*, **12**, 157–187.

11. Philander, S. G. H., Yamagata, T. & Pacanowski, R. C. 1984 Unstable air-sea interactions in the tropics. *J. Atmos. Sci.*, **41** (4), 604–613.

12. Rowley, C. & Ginis, I. 1999 Implementation of a mesh movement scheme in a multiply nested ocean model and its application to air?sea interaction studies. *Mon. Weather Rev.*, **127**, 1879–1896.

13. Spall, M. A. & Holland, W. R. 1991 A nested primitive equation model for oceanic applications. *J. Phys. Oceanogr.*, **21**, 205–220.